

TECHNICAL REPORT 1972
September 2008

**Wideband Multiport Matching
Phase I: Single-Feed
Multiport Antennas**

J. C. Allen
J. Rockway
D. Arceo

Approved for public release;
distribution is unlimited.

SSC San Diego

TECHNICAL REPORT 1972
September 2008

Wideband Multiport Matching Phase I: Single-Feed Multiport Antennas

J. C. Allen
J. Rockway
D. Arceo

Approved for public release;
distribution is unlimited.



*SPAWAR
Systems Center
San Diego*

SSC San Diego
San Diego, CA 92152-5001

SSC SAN DIEGO
San Diego, California 92152-5001

M. T. Kohlheim, CAPT, USN
Commanding Officer

C. A. Keeney
Technical Director

ADMINISTRATIVE INFORMATION

This report originated in the In-House Laboratory Independent Research (ILIR) Program of SPAWAR Systems Center San Diego and the Conformal Antennas Integration and Demonstration Program of the Office of Naval Research (ONR).

Released by
J. H. Meloling, Head
Applied Electromagnetics
Branch

Released under authority of
S. D. Russell, Head
Advanced Systems and
Applied Sciences Division

This is a work of the United States Government and therefore is not copyrighted. This work may be copied and disseminated without restriction. Many SSC San Diego public release documents are available in electronic format at <http://www.spawar.navy.mil/sti/publications/pubs/index.html>.

EXECUTIVE SUMMARY

Impedance matching is a canonical problem in electrical engineering. The problem is to maximize power flowing from a generator to a load with an adroit design of a matching network. Typically, matching problems use a single-port load. In contrast, this report develops matching for a load with multiple ports. The specific multiport load is a three-wire antenna. Each wire has a feed port so that the load is a 3-port. The matching problem is to find a matching network that maximizes power flow from a single feed to all three ports across a wide frequency band (100–700 MHz). Unexpectedly, several theoretical matching multiports were found that gave excellent wideband performance. Consequently, this serendipitous result opens several directions of opportunity.

One direction aims at enhancing the antenna’s wideband performance. Understanding the physical phenomenon of coupling between the wires, the physical geometry of the wires, and a Pareto theory for maximal bandwidth and minimal size are all significant research topics. Another direction aims at the matching networks because of the gaps in theory and practical design. Specific and detailed formulation of these research opportunities is made explicit in this report.

Contents

Executive Summary	iii
1 Why Multiport Matching?	1
2 Notation	4
3 The Three-Wire Antenna	6
4 The Direct Connection	11
5 Multiport Matching	14
6 Channelized Multiports	25
7 Exploiting Multiport Coupling	31
7.1 What are the theoretical limits of multiport matching?	31
7.2 What are the optimal multiport matching circuits?	33
7.3 How effective is decoupling?	33
7.4 What are the multiport ladder circuits?	34
7.5 How critical is multiport matching for MIMO?	35
7.6 Multiport Antenna System Optimization	37
References	39
A Characteristic Modes of the Three-Wire Antenna	A-1
B Lumped, Lossless N-Ports	B-1

List of Figures

1	Matching and decoupling schematic [37] © IEEE 2008.	2
2	6-port decoupling and matching [41] © IEEE 2006.	2
3	4-port matching with a single feed at Port 1.	2
4	Cascade of a 2-port and load.	5
5	Center-fed dipoles.	6
6	Admittance matrix—normalized magnitudes.	9
7	Scattering Matrix.	10
8	4-port matching; direct connection.	11
9	2-port matching of the direct connection.	11
10	Transducer power gain of the direct connection.	12
11	Smith chart of the direct connection.	12
12	Matching the direct connection.	13
13	Scattering waves for a 3-port.	14
14	Unmatched Gain.	16
15	Matching 4 port.	17
16	$d = 4$ matching over 100–700 MHz.	21
17	$d = 4$ matching over 140–700 MHz.	21
18	$d = 3$ matching over 140–700 MHz.	22
19	$d = 2$ matching over 140–700 MHz.	22
20	$d = 1$ matching over 140–700 MHz.	23
21	$d = 0$ matching over 140–700 MHz.	23
22	Matching with channelized 2-ports.	25
23	Simple channelized 2-ports.	25
24	Channelized 2-ports (shunt inductance)	27
25	Power trivider.	28
26	Power trivider matching 140–700 MHz.	29
27	Power trivider matching 300–600 MHz.	29
28	Power trivider matching 270–700 MHz.	30
29	Shunts between ports.	34
30	MIMO matching networks [25] © IEEE 2006.	35
31	MIMO receiver and matching network [26] © IEEE 2005.	36
32	Antenna system (single feed, port loading).	37
A-1	Center-fed Dipoles: 1/4, 1/2, and 1 meter in length	A-1
A-2	Impedance matrix at 150 MHz.	A-2
A-3	Eigencurrents at 150 MHz.	A-4
A-4	Eigencurrents at 300 MHz.	A-5

A-5	Eigencurrents at 600 MHz.	A-6
A-6	Eigencurrents at 450 MHz.	A-7
B-1	State-space representation of a passive, lumped N -port.	B-3

List of Tables

1	Notation.	4
2	Dipole specifications (meters).	6
3	MININEC wire models (millimeters).	7
4	Matching with $U^+(4, d)$ over 140–700 MHz.	24

1 Why Multiport Matching?

Impedance matching is a ubiquitous problem in electrical engineering. The standard matching problem searches for a 2-port that maximizes the power transfer from a generator to a load. Increasing bandwidth in communication systems, the integration of many functions on a chip, and multifunction antennas all lead to the problem of *multiport* matching. In general, when a generator and a load are multiports, the connecting matching network must also be a multiport.

Multiport matching assumes the ports of the load are coupled. Otherwise, uncoupled ports reduces matching to a collection of standard 2-port matching problems. A multiport antenna provides a splendid case study. When antenna arrays are spaced closer than half a wavelength ($\lambda/2$), mutual coupling effects emerge [38]:

When using multiple antenna elements for diversity implementation on small personal communications devices, the resulting closely spaced antenna elements exhibit the well-known mutual coupling ... [that] alters both their terminal impedance and radiation pattern characteristics. These changes obviously impact the diversity performance of the multiantenna system.

A powerful design approach is the emerging *port decoupling* [9]:

[port decoupling] involves a modal feed network which makes use of the orthogonality of the eigenmodes of the array to achieve decoupling. The input ports to the feed network and array combination can then be matched independently.

Figure 1 illustrates this decoupling and single-channel matching approach. Figure 2 shows a 6-port matching circuit where the decoupling and matching have been merged into a nicely interconnected multiport. Figure 3 shows a matching problem where a 3-port antenna is powered by a single feed. The 4-port matching networks will exploit the mutual coupling to attain a wideband antenna.

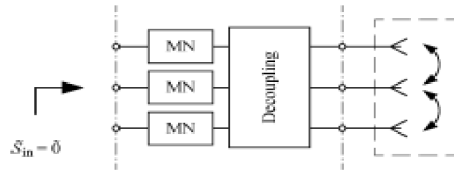


Figure 1: Matching and decoupling schematic [37] © IEEE 2008.

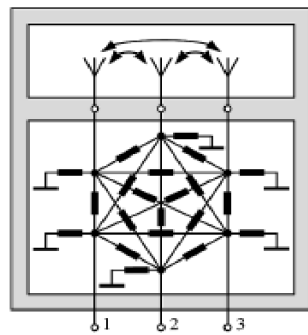


Figure 2: 6-port decoupling and matching [41] © IEEE 2006.

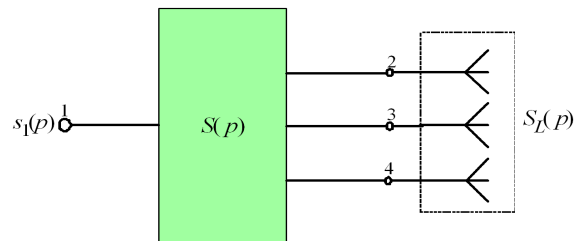


Figure 3: 4-port matching with a single feed at Port 1.

Section 3 describes the three-wire antenna, the three feed points, and the computation of its 3×3 admittance matrix over 100–700 MHz. This admittance matrix shows the resonances of the wires and the coupling between the wires.

Section 4 starts the matching process by directly connecting the three feed points to a common terminal. Thus, the three-wire antenna is turned into a standard single-port antenna amenable to 2-port matching. Unfortunately, this direct connection has a terrible Voltage Standing Wave Ratio (VSWR) over 100–700 MHz. The smallest VSWR attainable by *any* matching 2-port—regardless of the number of components and topology—exceeds 22. Only 17% of the power is delivered to the antenna—the remaining 83% is reflected back to the feed. Multiport matching improves this power delivery.

Section 5 matches of the three-wire antenna over the class of 4-ports shown in Figure 3. The matching results are excellent: the VSWR is less than 2.7 over 140–700 MHz. This multiport matching network delivers 79% of power to the antenna; only 21% is reflected back to the feed. This improvement of this wide-band VSWR motivated this exploration of multiport matching.

Section 6 straddles the preceding matching topologies by matching with a “channelized” 4-port—each port of the antenna is connected to its own matching 2-port. The preliminary results show that this “semi-direct” connection is not as viable, and the cross-coupling in the full multiport is necessary for a wideband match. This observation again raises questions regarding a physical understanding of multiport matching. Section 7 organizes these results into a collection of research topics:

- Developing H^∞ bounds to compute absolute matching performance
- Extracting a circuit from the general multiports
- Considering ladder-like multiport topologies
- Understanding the role of coupling and matching
- Other multiport matching applications

Appendix A offers an in-depth description of the resonances of the three-wire using *characteristic modes*. Appendix B reviews the necessary background on the lumped, lossless multiports used for matching.

2 Notation

Table 1 lists common notation. The last three entries are the scattering, impedance, and admittance matrices. The implicit assumptions when using these matrices is the existence and linear relationship of the currents and voltages [28]. For example, the admittance matrix Y of a three-port links the current and voltage vectors as

$$\begin{bmatrix} i_1 \\ i_2 \\ i_3 \end{bmatrix} = \begin{bmatrix} y_{11} & y_{12} & y_{13} \\ y_{21} & y_{22} & y_{23} \\ y_{31} & y_{32} & y_{33} \end{bmatrix} \begin{bmatrix} v_1 \\ v_2 \\ v_3 \end{bmatrix}.$$

Table 1: Notation.

symbol	Description
\mathbb{R}	Real numbers
\mathbb{C}	complex plane
\mathbb{C}_+	open right half complex plane
j	positive square root of -1
p	complex frequency: $p = \sigma + j\omega$
σ	neper frequency (nepers per second)
ω	radial frequency (radians per second)
I_N	$N \times N$ identity matrix
S	scattering matrix (unitless)
Y	admittance matrix (Siemens)
Z	impedance matrix (ohms)

Figure 4 illustrates the *cascade* of a 2-port with scattering matrix

$$S = \begin{bmatrix} s_{11} & s_{12} \\ s_{21} & s_{22} \end{bmatrix}$$

with Port 2 terminated in a load with reflectance s_L . The reflectance s_1 looking into Port 1 is

$$s_1 = \mathfrak{F}(S, s_L) := s_{11} + s_{12}s_L(1 - s_{22}s_L)^{-1}s_{21}.$$

When the dependence on the complex frequency p must be made explicit, the notation takes the form

$$\begin{aligned} s_1(p) &= \mathfrak{F}(S, s_L; p) \\ &:= s_{11}(p) + s_{12}(p)s_L(p)(1 - s_{22}(p)s_L(p))^{-1}s_{21}(p). \end{aligned}$$

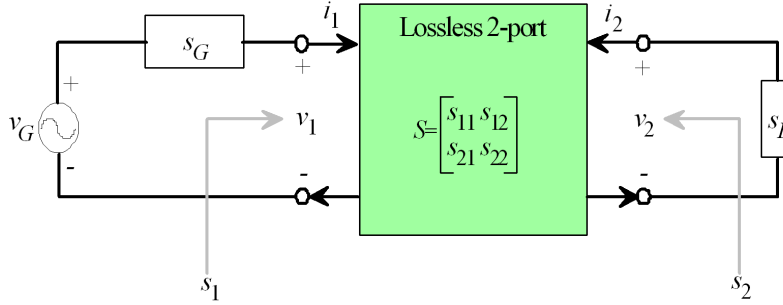


Figure 4: Cascade of a 2-port and load.

Let a multiport have a scattering matrix with a block structure

$$S = \begin{bmatrix} S_{11} & S_{12} \\ S_{21} & S_{22} \end{bmatrix}.$$

Let S_{11} be an $M \times M$ scattering matrix that corresponds to Ports 1, 2, ..., M . Let S_{22} be an $N \times N$ scattering matrix that corresponds to the remaining N ports. If these remaining N ports are terminated in an N -port load with scattering matrix S_L , the scattering matrix looking into Ports 1, 2, ..., M is

$$\mathfrak{F}(S, S_L) := S_{11} + S_{12}S_L(I_N - S_{22}S_L)^{-1}S_{21},$$

where I_N denotes the $N \times N$ identity matrix.

3 The Three-Wire Antenna

An arbitrary three-wire antenna was chosen to investigate the value of multiport matching. Figure 5 shows that the antenna consists of three closely spaced center-fed vertical dipoles operating over 100–700 MHz.

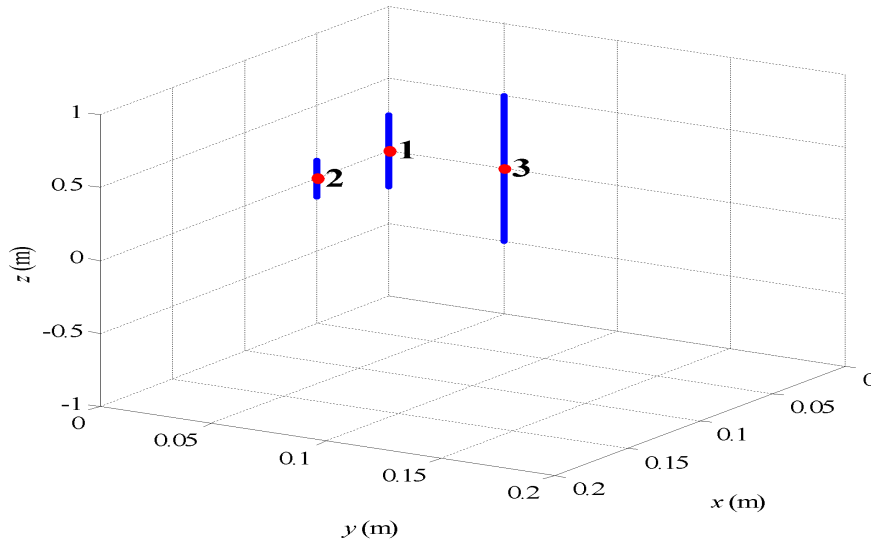


Figure 5: Center-fed dipoles.

The dipole lengths and resonant frequencies are listed in Table 2. Comparing the wavelengths to the antenna distances justifies “closely spaced” as a descriptor.

Table 2: Dipole specifications (meters).

Wire	x	y	Length
1	0.00	0.00	0.50
2	0.05	0.00	0.25
3	0.00	0.05	1.00

The admittance matrix of this three-wire antenna provides insight into its multiport response. Specifically, the admittance matrix shows the *resonant*

and *mutual coupling* frequencies. It suffices to define¹ these frequencies from the local maxima of admittance’s magnitude. The admittance matrix relates the feed-point voltages to the feed-point currents measured at Ports 1, 2, and 3 of Figure 5:

$$\begin{bmatrix} i_1 \\ i_2 \\ i_3 \end{bmatrix} = \begin{bmatrix} y_{11} & y_{12} & y_{13} \\ y_{21} & y_{22} & y_{23} \\ y_{31} & y_{32} & y_{33} \end{bmatrix} \begin{bmatrix} v_1 \\ v_2 \\ v_3 \end{bmatrix}.$$

The feed point admittance were calculated using Version 14 of the *Expert MININEC Broadcast Professional* [32]. This software is an advanced engineering tool for the design and analysis of wire antennas. The wire antennas are assumed to be a collection of arbitrary thin, straight wires in free space or over a ground plane. A method of moments algorithm solves for the current distribution on the wires. The solution for current distribution is based on the numerical solution of an integral equation representation of the electric fields [33]. The process of solution begins with thin-wire assumptions [36]:

W-1 Antennas must be modeled as a group of one or more straight wires.

W-2 The wire radius is very small with respect to the wire length.

W-3 Parallel wires should be several wire diameters or more apart.

W-4 The radius is very small with respect to segment lengths.

Table 3 tabulates the dipole’s lengths, radii, and segment lengths. Compared to the wavelength $\lambda = 0.43$ meters at 700 MHz, this antenna model is within MININEC assumptions W-1, W-2, W-3, and W-4.

Table 3: MININEC wire models (millimeters).

Wire	Length	Radius	Segment	Separation
1	500	1	25	50
2	250	1	25	50
3	1,000	1	25	50

¹Subsequent reports will include a multiport generalization of resonance and anti-resonance defined on the Smith chart.

The electric field is determined by the vector magnetic potential and the scalar electric potential. The two potentials are calculated from potential integrals that are solutions of the Helmholtz vector and scalar wave equations. The integrands of the potential integrals are the wire current and wire charge distributions. Because wires are thin, the currents are axially directed (i.e., no circumferential currents on the wires). The current and charge are linked by the equation of continuity. *Expert MININEC Broadcast Professional* assumes the following boundary condition:

TE-0 The tangential electric field at the surface of a perfect conductor is zero.

Because the wires are assumed to be thin, this assumption forces the total axial electric field on the wire to zero. The three sources of the tangential electric field on the wire are:

TE-1 currents and charges on the wires and on nearby wires,

TE-2 incoming waves from distance or nearby radiators,

TE-3 local sources of electric field on the wire.

The local sources are voltage sources or current sources that connect to the wires. By summing the tangential electric field components at each segment on the wire antenna and enforcing the zero total value, an integral representation for the currents and charges is obtained.

The electric field integral equation is solved in *Expert MININEC Broadcast Professional* by the method of moments. Basis functions are chosen to represent the unknown currents (i.e., triangular basis functions). Testing functions are chosen to enforce the integral equation on the surface of the wires. These basis and testing functions yield a matrix approximation of the integral equations. If this matrix is inverted and multiplied by the local sources of electric field, the complex magnitudes of the current basis functions are derived. All antenna performance parameters can be determined from the derived current distribution, including the feed point admittance.

Figure 6 plots the admittance matrix as a function of frequency. Each (m, n) subplot plots the magnitude of its corresponding *normalized* admittance $|y_{m,n}|$. The antenna resonances are prominent features of the port admittances $y_{1,1}$, $y_{2,2}$, and $y_{3,3}$ along the main diagonal: The 0.5-meter dipole has $|y_{1,1}|$ showing a peak near 300 MHz. The 0.25-meter dipole has $|y_{2,2}|$

peaking near 600 MHz. The 1-meter dipole has $|y_{3,3}|$ peaking near 150 MHz and 450 MHz.

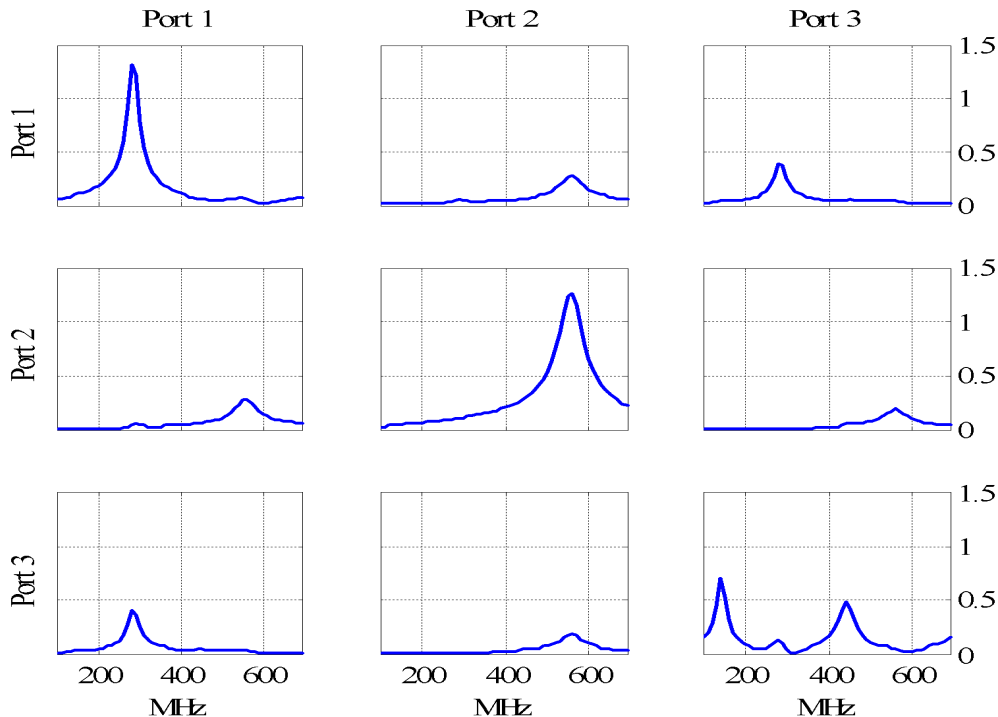


Figure 6: Admittance matrix—normalized magnitudes.

The plot also shows both the coupling and reciprocity ($Y = Y^T$) between the dipoles. For example, the voltage v_1 across Port 1 to 0.5-meter dipole also produces currents from Port 2 (the 0.25-meter dipole) at 600 MHz and Port 3 (the 1-meter dipole) at 300 MHz. Likewise, voltage v_2 across Port 2 to the 0.25-meter dipole produces currents from Port 1 (the 0.5-meter dipole) and Port 3 (the 1-meter dipole) at 600 MHz. Finally, the voltage v_3 across Port 3 feeds to the 1-meter dipole currents from Port 1 at 300 MHz and in Port 2 at 600 MHz. Consequently, the admittance plot does reveal some of the resonances and mutual couplings.

Figure 7 plots the scattering matrix the three-wire antenna as a function of frequency f . For $f < 200$ MHz, the reflectances are plotted in black. For $f > 200$ MHz, the reflectances are plotted in blue. The Smith chart reveals the resonances of the input ports: A *resonant frequency* ω_\times is defined where $s(j\omega_\times)$ crosses the real axis in the upward direction. An *anti-resonant*

frequency ω_{\otimes} is defined where $s(j\omega_{\otimes})$ crosses the real axis in the downward direction [43]. For example, $s_{3,3}(j\omega)$ explains that two large spikes at 150 and 450 MHz in the admittance plot are resonant frequencies while the spike at 300 MHz is an anti-resonant frequency.

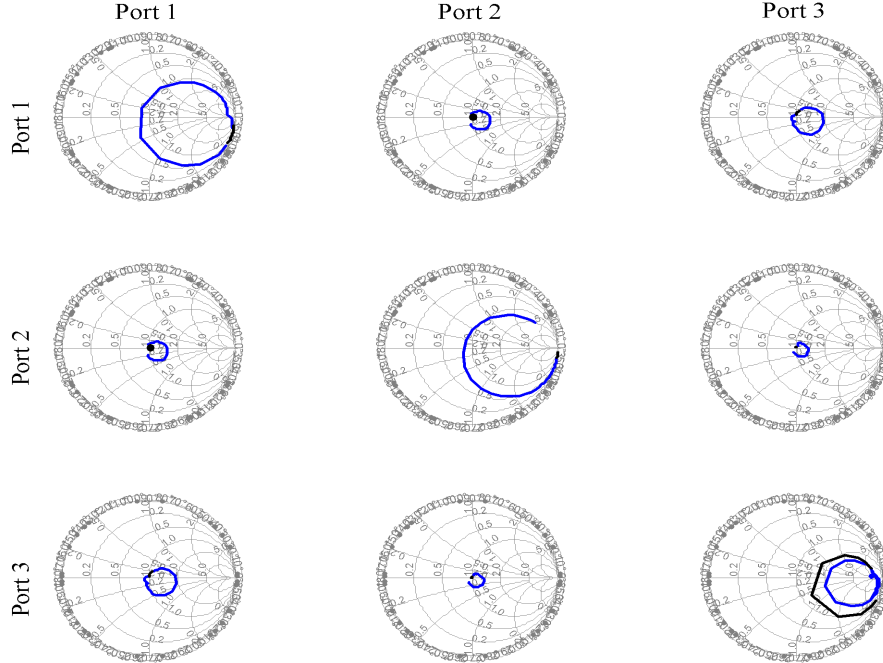


Figure 7: Scattering Matrix.

Finally, because this scattering matrix is the “object under discussion,” the limitations of the antenna model are made explicit. First, the limitations of MININEC are recognized [36] and a convergence study was not performed [33]. Second, the dipole’s lengths were chosen for convenience. A more judicious choice of dipole lengths will produce more resonances in 100–700 MHz. Third, the sensitivity of this antenna to physical perturbations has not been studied. Nevertheless, the wavelength and the physical dimensions argue that this three-wire antenna is “good enough” as a multiport matching exemplar.

4 The Direct Connection

This section starts the matching process using the *direct connection* as a baseline case. Figure 8 is a schematic of the direct connection. The green box is the matching 4-port that simply wires all three ports of the antenna to the single feed.

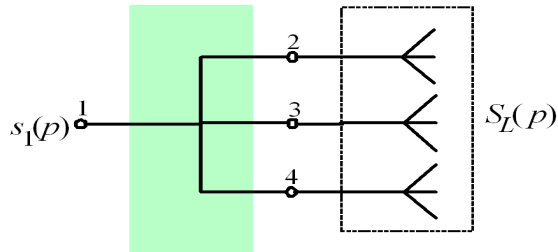


Figure 8: 4-port matching; direct connection.

This direct connection converts the 3-port antenna into a 1-port antenna amenable to standard matching as shown in Figure 9. Consequently, the performance obtained by matching this direct connection benchmarks the performance attained by the multiport matching networks.

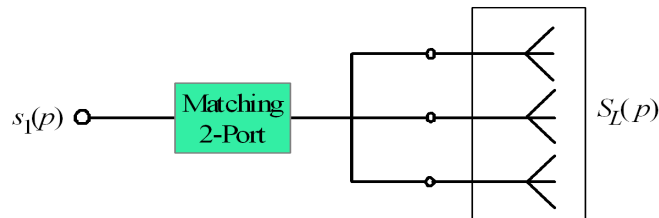


Figure 9: 2-port matching of the direct connection.

Figure 10 plots the transducer power gain of the direct connection:

$$G_T(j\omega) = 1 - |s_1(j\omega)|^2,$$

where $s_1(j\omega)$ is the reflectance looking into the feed to the antenna. In addition to the expected resonances near 150, 300, and 600 MHz, a resonance exists near 450 MHz. Appendix A shows that this resonance is on the long wire. Figure 11 plots the reflectance of the direct connection on the Smith chart. The number and location of these loops near the boundary of the Smith chart indicate that matching is difficult.

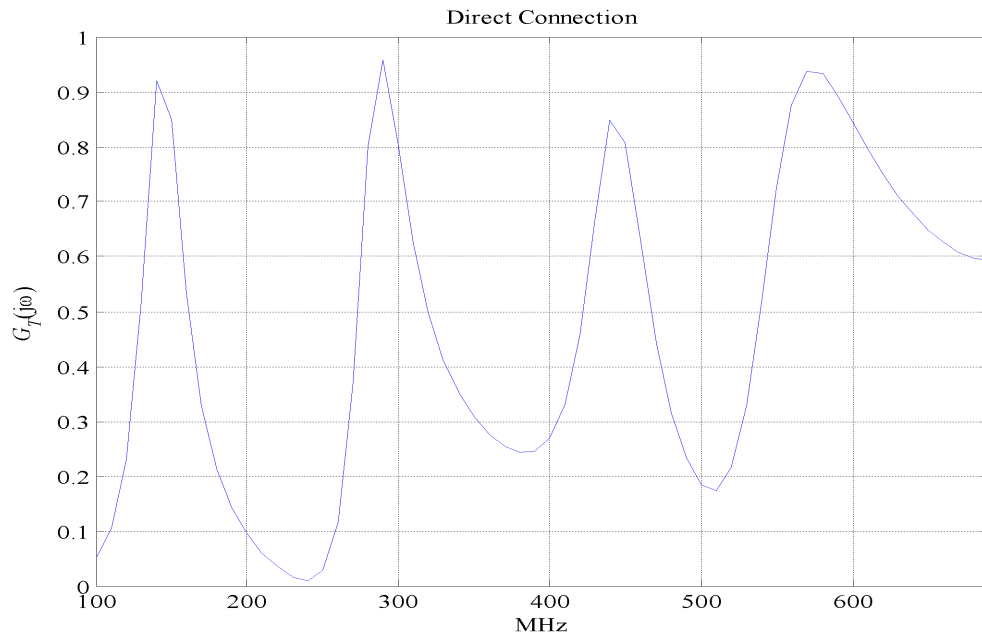


Figure 10: Transducer power gain of the direct connection.

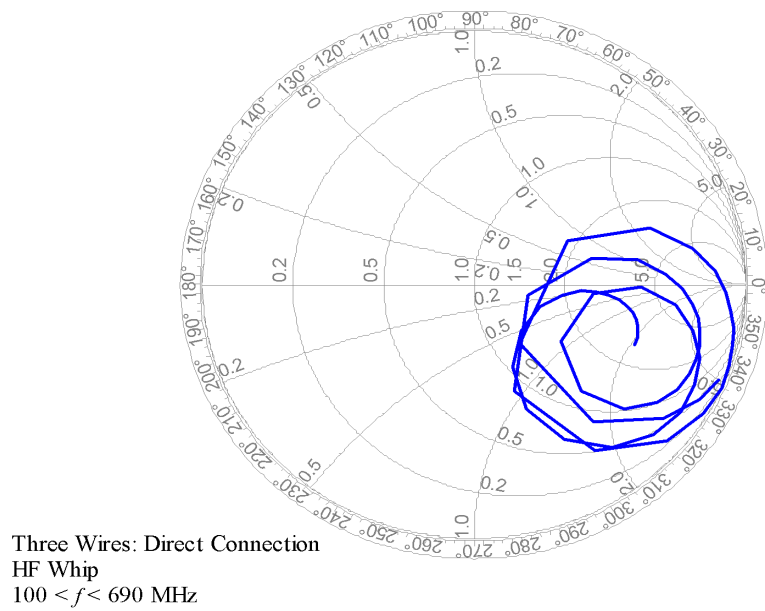


Figure 11: Smith chart of the direct connection.

Figure 12 shows the difficulty of matching the direct connection. The plot shows the matching performance of various classes of 2-ports connecting the feed point to a generator as shown in Figure 9. The vertical axis is the VSWR. The horizontal axis is the degree d of the matching 2-port and is equivalent to the number of lumped elements in the 2-port. The curve labeled “low-pass ladders” plots the VSWR as a function of the number of elements and attains a VSWR in excess of 25. The solid patch marks the H^∞ bound—the smallest VSWR attainable by any lossless 2-port. This VSWR exceeds 22 so that this direct connection is useless. Between these two plots lies the “state-space” curves. This curve plots the matching performance available from all lumped, lossless 2-ports of degree d . This matching class is reviewed in Appendix B and is the basis for the multiport matching in the next section.

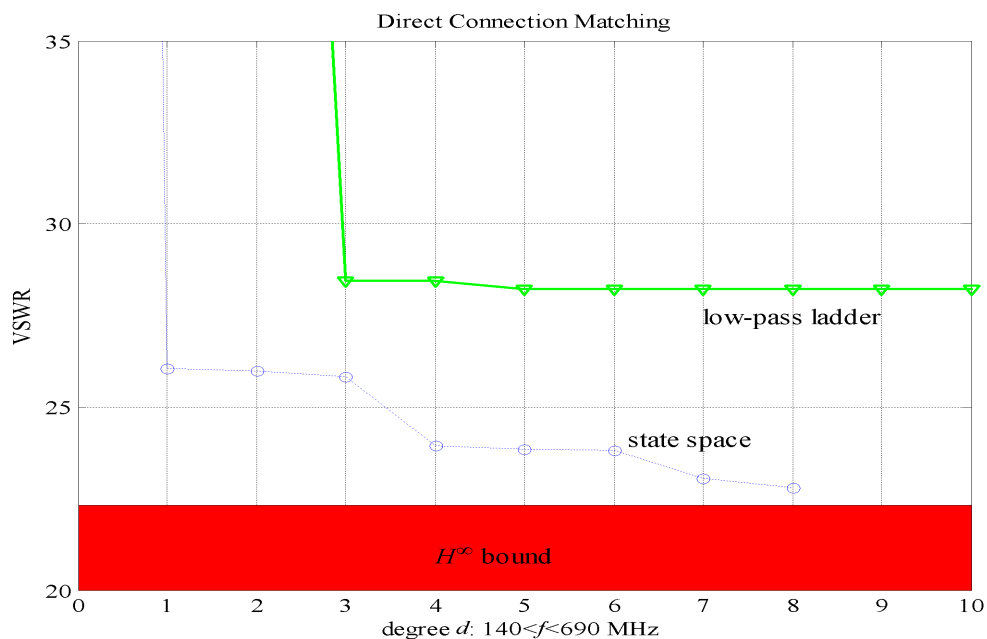


Figure 12: Matching the direct connection.

5 Multiport Matching

Figure 13 is a schematic showing the voltages, currents, and incident and reflected waves of a 3-port.

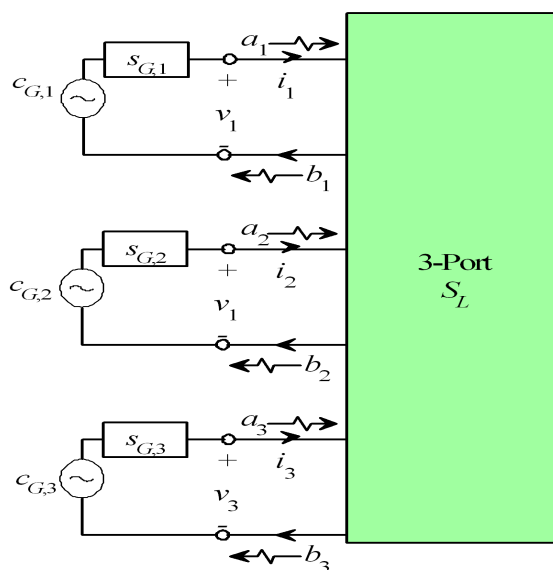


Figure 13: Scattering waves for a 3-port.

The *incident wave* [4, Eq. 4.25a], [5, page 234]

$$\mathbf{a} = \frac{1}{2}\{R_0^{-1/2}\mathbf{v} + R_0^{1/2}\mathbf{i}\}$$

and the *reflected wave* [4, Eq. 4.25b], [5, page 234]

$$\mathbf{b} = \frac{1}{2}\{R_0^{-1/2}\mathbf{v} - R_0^{1/2}\mathbf{i}\}$$

are defined with respect to the normalizing² matrix

$$R_0 = \begin{bmatrix} r_{0,1} & 0 & 0 \\ 0 & r_{0,2} & 0 \\ 0 & 0 & r_{0,3} \end{bmatrix}.$$

²Two accessible books on the scattering formalism are Baher [4] and Balabanian & Bickhart [5]. Baher omits the factor of 1/2 but carries this rescaling into the power definitions. Most other books use the *power-wave normalization* [14]: $\mathbf{a} = R_0^{-1/2}\{\mathbf{v} + Z_0\mathbf{i}\}/2$, where the normalizing matrix $Z_0 = R_0 + jX_0$ is diagonal with diagonal resistance $R_0 > 0$ and reactance X_0 .

This document always normalizes with respect to $r_0 = 50$ ohms:

$$R_0 = r_0 \begin{bmatrix} 1 & 0 & 0 \\ 0 & 1 & 0 \\ 0 & 0 & 1 \end{bmatrix} = r_0 I_3.$$

The *scattering matrix* $S_L(p)$ maps the incident signal $\mathbf{a}(p)$ to the reflected signal $\mathbf{b}(p)$:

$$\mathbf{b} = \begin{bmatrix} b_1 \\ b_2 \\ b_3 \end{bmatrix} = \begin{bmatrix} s_{11} & s_{12} & s_{13} \\ s_{21} & s_{22} & s_{23} \\ s_{31} & s_{32} & s_{33} \end{bmatrix} \begin{bmatrix} a_1 \\ a_2 \\ a_3 \end{bmatrix} = S_L \mathbf{a}.$$

The complex power³ delivered to the 3-port is [5, page 241]:

$$W(p) := \mathbf{v}(p)^H \mathbf{i}(p).$$

The average power delivered to the 3-port is [18, page 19], [25]:

$$P_L := \frac{1}{2} \Re[W] = \frac{1}{2} \{\mathbf{a}^H \mathbf{a} - \mathbf{b}^H \mathbf{b}\} = \frac{1}{2} \mathbf{a}^H \{I - S_L^H S_L\} \mathbf{a}. \quad (1)$$

The matrix $I - S_L^H S_L$ is called the *dissipation matrix* [10] or the *radiation matrix* [37]. The latter name is misleading because it implies that the power P_L that is delivered to the antenna is actually radiated. The eigen-decomposition of this matrix, which is equivalent to the eigen-decomposition of the scattering matrix S_L , is basic to matching [37]. If the 3-port consumes power ($P_L \geq 0$) for all its voltage and current pairs, the N -port is said to be passive. Because $\mathbf{v}(p)$ is the Fourier transform of the voltage vector $\mathbf{V}(t)$:

$$\mathbf{v}(p) = \int_{-\infty}^{\infty} e^{-j2\pi pt} \mathbf{V}(t) dt,$$

$\mathbf{v}(p)$ has units V/Hz. Likewise, $\mathbf{i}(p)$ has units A/Hz, so that $W(p)$ units of W/Hz². In comparison, both the incident wave \mathbf{a} and the reflected wave \mathbf{b} have units of $\sqrt{\text{W}}/\text{Hz}$ so that it makes sense to call

$$P_a = \mathbf{a}^H \mathbf{a}$$

³Baher uses [4, Eq. 2.17]: $W(p) = \mathbf{i}(p)^H \mathbf{v}(p)$. Gonzalez [18] power definitions require a “1/2”.

the *incident power* and

$$P_b = \mathbf{b}^H \mathbf{b}$$

the *reflected power*, respectively [5, page 227]. Optimal feed schemes are those that *minimize the reflected power*:

$$\min\{P_b(\mathbf{a}) : P_a = 1\}.$$

Equivalently, these optimal feed schemes are also solutions to the matrix norm problem:

$$\|I - S_L^H S_L\| = \max\{\mathbf{a}^H (I - S_L^H S_L) \mathbf{a} : \|\mathbf{a}\| = 1\}.$$

The physical interpretation of this feed scheme is that it maximizes the power delivered to the antenna subject to the constraint of unit incident power [37]. Figure 14 plots the norm of the dissipation matrix as a function of frequency.

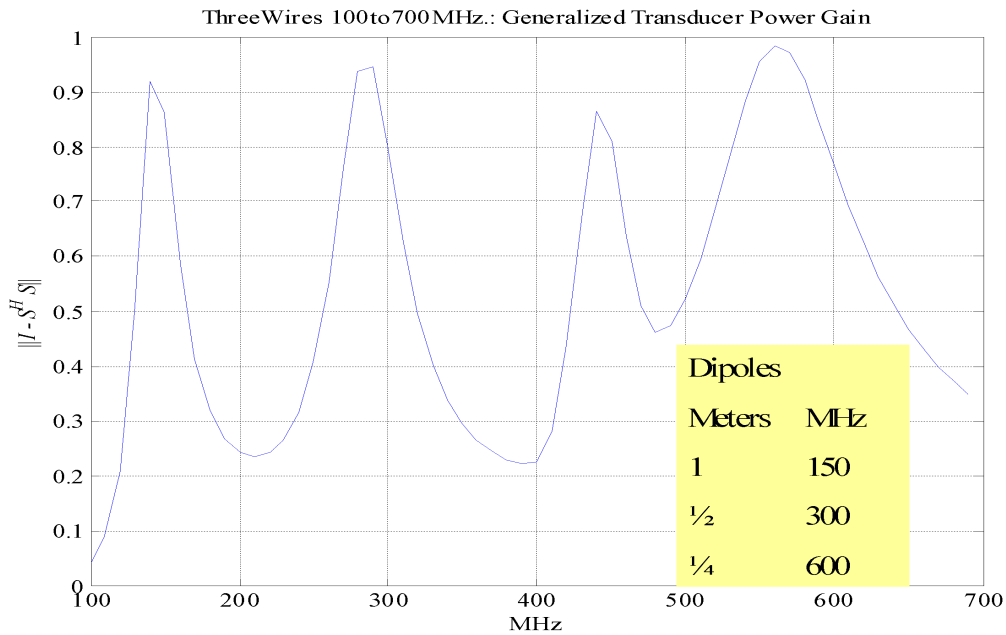


Figure 14: Unmatched Gain.

The matching network should map the generator's power to an output power that will be more useful at the load. The modification of power is generically called "gain." The matching problem requires gain computations, and we need the maximum power and mismatch definitions. The maximum power available from a generator is defined as the average power delivered by the generator to a conjugately matched load [18, Eq. 2.6.7]:

$$P_{G,\max} := P_G|_{s_1=\overline{s_G}} = \frac{|c_G|^2}{2}(1 - |s_G|^2)^{-1}.$$

The *transducer power gain* is [18, page 213]:

$$G_T := \frac{P_L}{P_{G,\max}} = \frac{\text{power delivered to the load}}{\text{maximum power available from the generator}}.$$

Lemma 1 *Figure 15 is a schematic of a 4-port that matches a generator looking into Port 1 to a 3-port load terminating Ports 2, 3, and 4.*

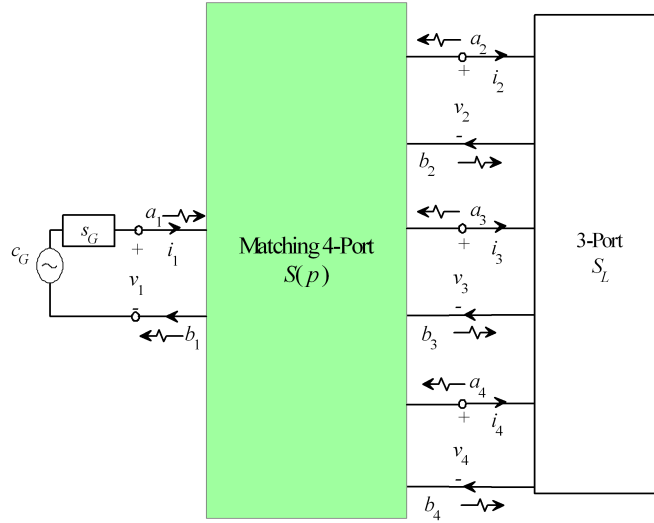


Figure 15: Matching 4 port.

The reflectance looking into Port 1 is

$$s_1 = s_{11} + S_{12}S_L(I_3 - S_{22}S_L)^{-1}S_{21}.$$

The transducer power gain is

$$G_T = \frac{1 - |s_G|^2}{|1 - s_G s_1|^2} S_{21}^H (I_3 - S_{22}S_L)^{-H} (I_3 - S_L^H S_L) (I_3 - S_{22}S_L)^{-1} S_{21}. \quad (2)$$

Proof: The first task is to link the power P_L delivered to the 3-port load (Equation 1) to the input a_1 . The 4-port scattering equations and the load reflectance are:

$$\begin{bmatrix} b_1 \\ \mathbf{b}_2 \end{bmatrix} = \begin{bmatrix} s_{11} & S_{12} \\ S_{21} & S_{22} \end{bmatrix} \begin{bmatrix} a_1 \\ \mathbf{a}_2 \end{bmatrix}; \quad S_L \mathbf{b}_2 = \mathbf{a}_2.$$

Eliminate \mathbf{a}_2 from the lower equation:

$$\mathbf{b}_2 = (I_3 - S_{22}S_L)^{-1}S_{21}a_1.$$

The power P_L delivered to the 3-port load is

$$P_L = \frac{1}{2} \bar{a}_1 S_{21}^H (I_3 - S_{22}S_L)^{-H} (I_3 - S_L^H S_L) (I_3 - S_{22}S_L)^{-1} S_{21} a_1.$$

A corresponding symmetry of the power relations exists at the input port. The reflectances at Port 1 and the generator are

$$b_1 = s_1 a_1; \quad a_1 = s_G b_1 + c_G.$$

Eliminate b_1 from the generator's equation:

$$(1 - s_G s_1) a_1 = c_G.$$

Substitute into the power P_L to the load:

$$P_L = \frac{1}{2} \frac{|c_G|^2}{|1 - s_G s_1|^2} S_{21}^H (I_3 - S_{22}S_L)^{-H} (I_3 - S_L^H S_L) (I_3 - S_{22}S_L)^{-1} S_{21}.$$

Dividing by the maximum gain available from the generator gives the result.

///

Lemma 1 is a simple algebraic statement that holds regardless of the passivity of the matching 4-port or the 3-port load. All that is required is that the inverses exist. A substantial simplification is possible when the matching 4-port is lossless.

Corollary 1 *Assume the schematic of Figure 15. Assume the 4-port is lossless:*

$$S^H S = I_4.$$

Assume the load $S_L(p)$ is strictly passive:

$$S_L^H S_L < I_3.$$

Assume the reflectance of the generator is zero:

$$s_G = 0.$$

The transducer power gain is

$$G_T = 1 - |s_1|^2. \quad (3)$$

The smallest transducer power gain over a frequency band Ω is denoted

$$\|G_T(s_G, S, S_L)\|_{-\infty, \Omega} := \min\{G_T(s_G, S, S_L; j\omega) : \omega \in \Omega\},$$

where the dependence on the generator's reflectance $s_G(p)$, the matching 4-port $S(p)$, and the load $S_L(p)$ is made explicit. The generator's reflectance $s_G(p)$ and the load $S_L(p)$ are fixed. The collection of matching 4-ports specified by the circuit designer is called the *designable* part and denoted \mathfrak{S} . The Single-Input Multiple-Output (SIMO) matching problem is to find lossless multiports from \mathfrak{S} that maximize the transducer power gain G_T over a frequency band Ω . Generalizing this SIMO matching problem for an N -port load is straightforward:

SIMO Matching: Given the generator's reflectance s_G , an N -port load $S_L(p)$ and a class \mathfrak{S} of lossless $(N + 1)$ -ports, maximize the transducer power gain:

$$\sup\{\|G_T(s_G, S, S_L)\|_{\Omega, -\infty} : S \in \mathfrak{S}\}.$$

A general matching class consists of all the lumped, lossless N -ports of degree d . This class is denoted by $U^+(N, d)$ and described in detail in Appendix B. Physically, $U^+(N, d)$ represents *all* the N -ports that can be synthesized with at most d *lumped* elements—inductors and capacitors—connected only by wires, transformers, and gyrators.

Mathematically, $U^+(N, d)$ consists of all $N \times N$ scattering matrices $S(p)$ that are rational functions analytic and bounded on the open right half of the complex plane, real on the real axis,

$$S(p) = \overline{S(\bar{p})},$$

unitary on the imaginary axis

$$S(j\omega)^H S(j\omega) = I_N,$$

and have Smith-McMillan degree

$$\text{deg}_{\text{SM}}[S(p)] \leq d.$$

Figures 16, 17 18, 19, 20, and 21 match the 3-port antenna from $U^+(4, d)$. The optimization problem is the SIMO Matching:

$$\sup\{\|G_T(s_G, S, S_L)\|_{\Omega, -\infty} : S \in U^+(4, d)\}.$$

Figure 16 plots the 4-port matching over the full frequency band 100–700 MHz. The blue curve plots the unmatched gain from Figure 14. The green curve plots the gain obtained by matching over $U^+(4, d)$ when $d = 4$. The transducer power gain is improved from -14 dB to -3 dB but the poor response of the antenna near 100 MHz limits the performance. Figure 17 verifies this statement by matching from the $d = 4$ multiports but limiting the frequency band to 140–700 MHz. Excellent matching performance is obtained with the nearly flat gain function. This “flatness” of the gain at optimum is characteristic of H^∞ theory.

Conjecture: SIMO matching solutions are characterized by flat gain as $d \rightarrow \infty$.

Figure 18 shows that matching with $d = 3$ still has a nearly flat response to support the conjecture. Figures 19, 20, and 21 match with $d = 2, 1, 0$ with only a 0.6-dB decrease in performance. However, at these suboptimal solutions, an “equal-ripple” is emerging.

Conjecture: SIMO matching solutions are characterized by an “equal-ripple” gain for $d < \infty$.

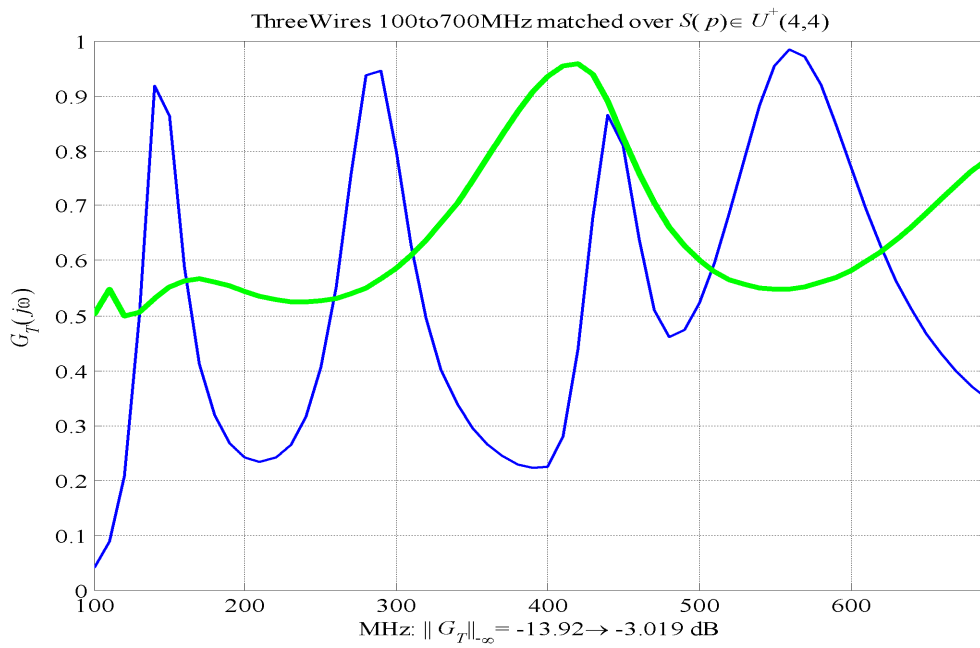


Figure 16: $d = 4$ matching over 100–700 MHz.

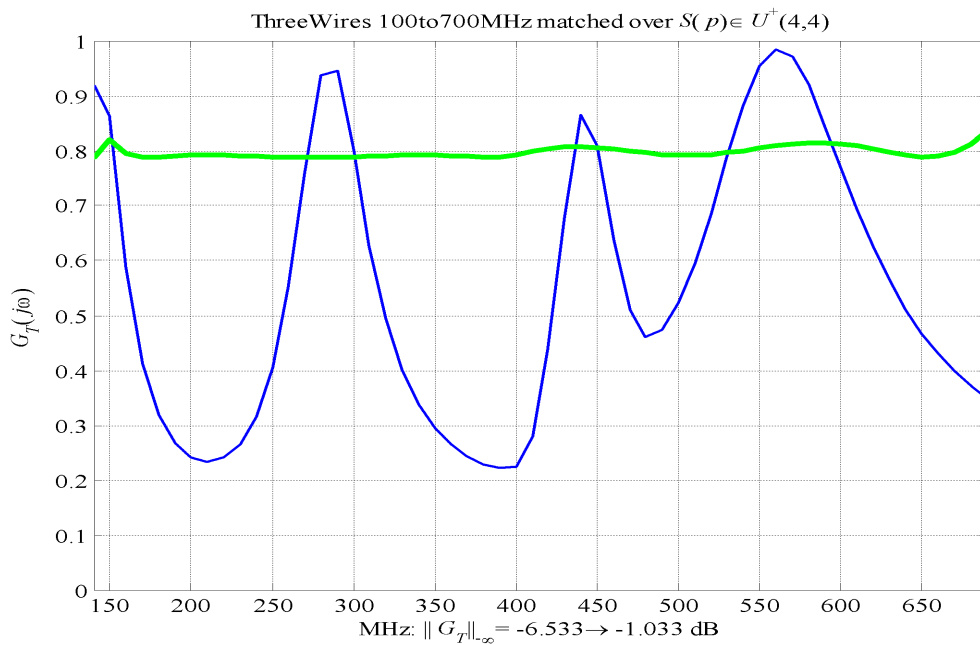


Figure 17: $d = 4$ matching over 140–700 MHz.

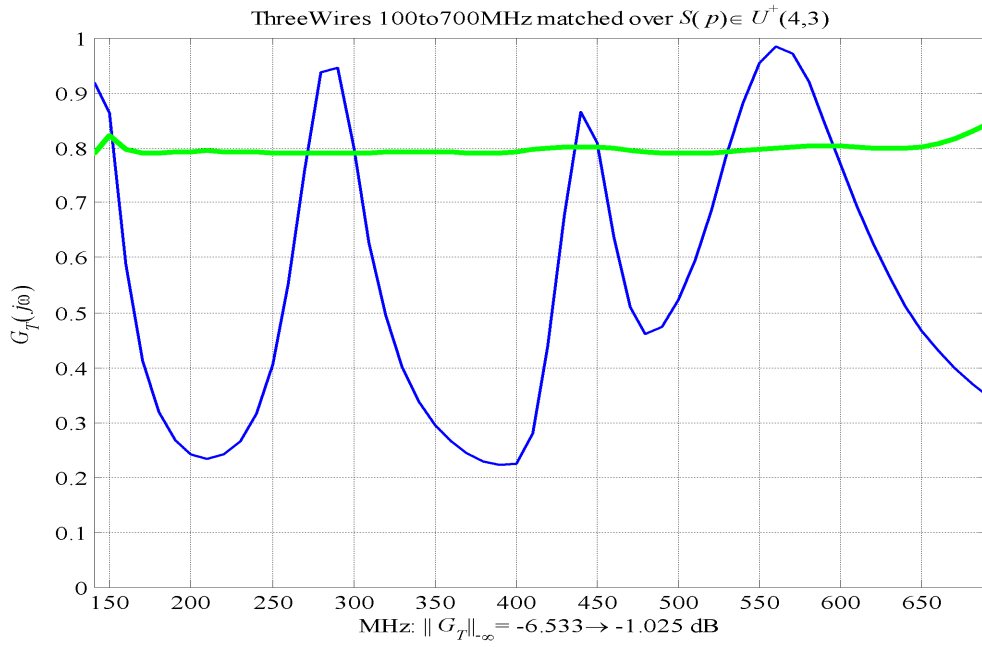


Figure 18: $d = 3$ matching over 140–700 MHz.

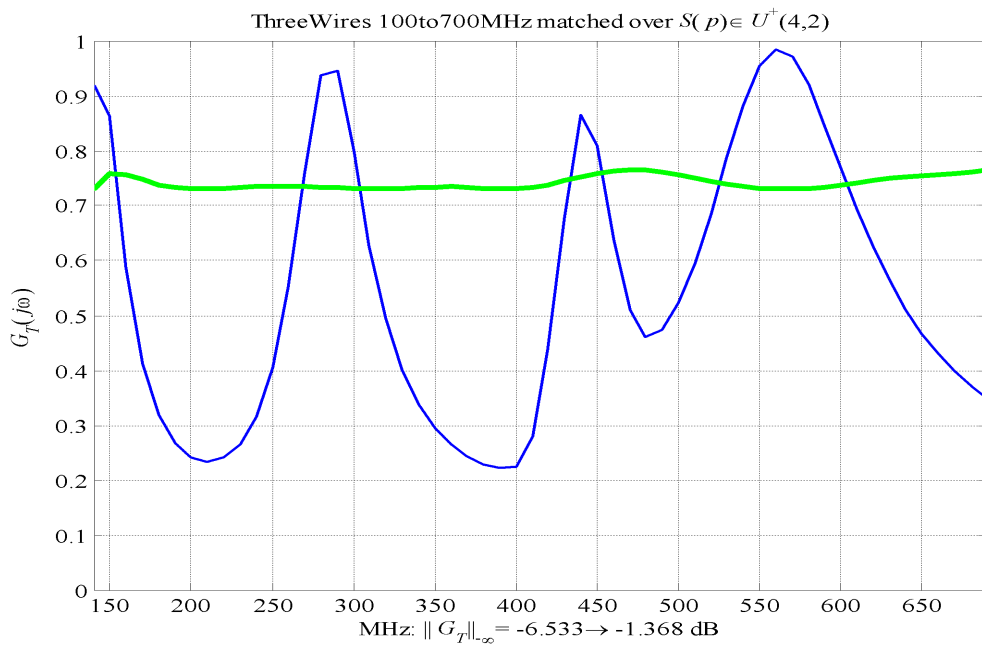


Figure 19: $d = 2$ matching over 140–700 MHz.

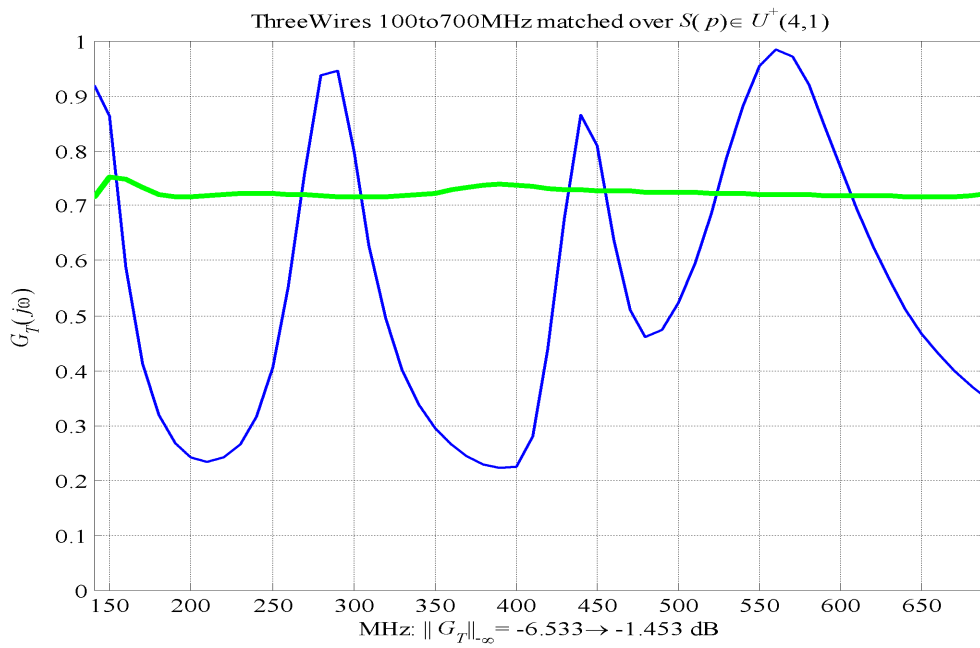


Figure 20: $d = 1$ matching over 140–700 MHz.

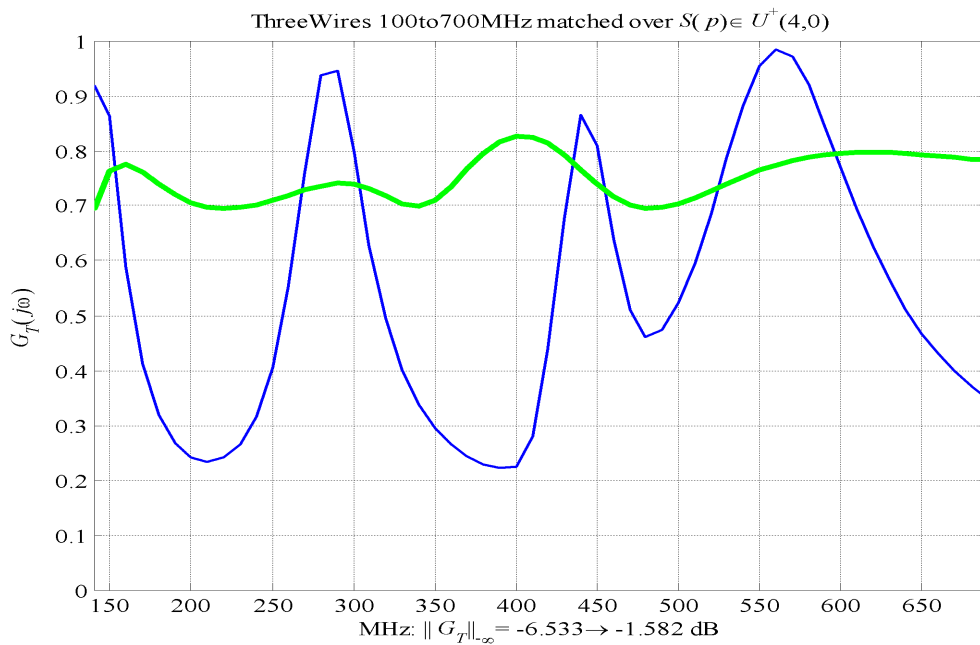


Figure 21: $d = 0$ matching over 140–700 MHz.

Table 4 tabulates the matching performance as a function of degree. The rolling off of the matching with increasing degree and the flatness of the gain support the conjecture that -1 dB is a reasonable matching bound. Indeed, it is the flatness of the gain that is *characteristic* of the H^∞ theory [21]. This flat gain leads to the excellent research question: *How much of the H^∞ theory carries over to the SIMO matching problem?*

Table 4: Matching with $U^+(4, d)$ over 140–700 MHz.

d	Gain (dB)	VSWR
0	-1.582	3.4696
1	-1.453	3.2849
2	-1.368	3.1651
3	-1.025	2.6935
4	-1.033	2.7043

What is also intriguing about Table 4 is that the greatest improvement in matching is obtained by the non-reactive 4-port for $d = 0$. The associated scattering matrix is

$$S = \begin{bmatrix} 0.5748 & -0.1638 & -0.3528 & -0.7199 \\ 0.4973 & 0.8192 & 0.2754 & 0.0757 \\ 0.4024 & -0.5057 & 0.7604 & 0.0637 \\ 0.5103 & -0.2150 & -0.4706 & 0.6870 \end{bmatrix}.$$

This scattering matrix is not reciprocal but exhibits a non-zero *gyrator rank* discussed in Appendix B:

$$2 = g[S] = \frac{1}{2} \text{rank}(S - S^T).$$

That is, a non-reactive 4-port must contain at least 2 gyrators. Therefore, an excellent research question asks: *What multiport matching is possible with reciprocal (gyrator-free) multiports?*

6 Channelized Multiports

The excellent matching obtained by the general multiports $U^+(4, d)$ raises an interesting question: are these multiports masking the simpler matching topology of channelized 2-ports? Figure 22 is a schematic of the channelized 2-ports.

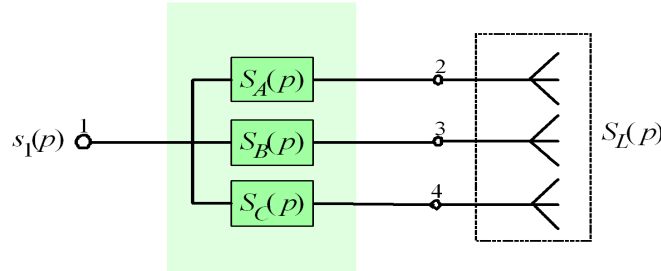


Figure 22: Matching with channelized 2-ports.

The matching 4-port is obtained as the compression of a 6-port. Figure 23 is a schematic of the 6-port that ties Ports 1, 3, and 5 together.

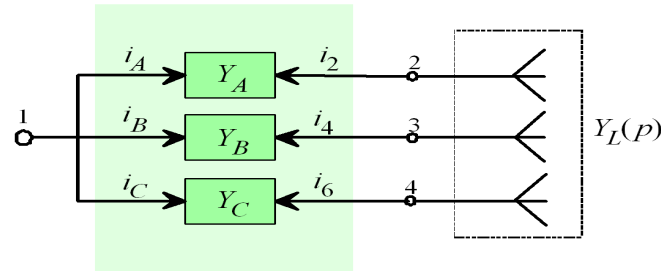


Figure 23: Simple channelized 2-ports.

The 6-port has admittance matrix

$$Y_A \oplus Y_B \oplus Y_C = \begin{bmatrix} y_{A,11} & y_{A,12} & 0 & 0 & 0 & 0 \\ y_{A,21} & y_{A,22} & 0 & 0 & 0 & 0 \\ 0 & 0 & y_{B,11} & y_{B,12} & 0 & 0 \\ 0 & 0 & y_{B,21} & y_{B,22} & 0 & 0 \\ 0 & 0 & 0 & 0 & y_{C,11} & y_{C,12} \\ 0 & 0 & 0 & 0 & y_{C,21} & y_{C,22} \end{bmatrix}.$$

Using the labeling in Figure 23, the current vector for the 4-port is the compression of the current vector for the 6-port:

$$\begin{bmatrix} i_1 \\ i_2 \\ i_3 \\ i_4 \end{bmatrix} = \begin{bmatrix} 1 & 0 & 1 & 0 & 1 & 0 \\ 0 & 1 & 0 & 0 & 0 & 0 \\ 0 & 0 & 0 & 1 & 0 & 0 \\ 0 & 0 & 0 & 0 & 0 & 1 \end{bmatrix} \begin{bmatrix} i_A \\ i_2 \\ i_B \\ i_4 \\ i_C \\ i_6 \end{bmatrix}.$$

Let E denote the transpose of this compression matrix for the current vectors. Matrix E is the *expansion matrix* for the voltage vectors:

$$\begin{bmatrix} v_A \\ v_2 \\ v_B \\ v_4 \\ v_C \\ v_6 \end{bmatrix} = \begin{bmatrix} 1 & 0 & 0 & 0 \\ 0 & 1 & 0 & 0 \\ 1 & 0 & 0 & 0 \\ 0 & 0 & 1 & 0 \\ 1 & 0 & 0 & 0 \\ 0 & 0 & 0 & 1 \end{bmatrix} \begin{bmatrix} v_1 \\ v_2 \\ v_3 \\ v_4 \end{bmatrix}.$$

The admittance matrix Y for the 4-port is the full 6-port admittance matrix multiplied on the left by the current compression matrix and on the right by the voltage expansion matrix:

$$\begin{aligned} Y &= E^T \{Y_A \oplus Y_B \oplus Y_C\} E \\ &= \begin{bmatrix} y_{A,11} + y_{B,11} + y_{C,11} & y_{A,12} & y_{B,12} & y_{C,12} \\ y_{A,21} & y_{A,22} & 0 & 0 \\ y_{B,21} & 0 & y_{B,22} & 0 \\ y_{C,21} & 0 & 0 & y_{C,22} \end{bmatrix}. \end{aligned}$$

The preliminary results matching with this channelized multiport are negative but intriguing. Figure 24 displays the matching that shunt inductors obtained over 140–700 MHz. The blue line is the gain of the direct connection. The green line is the gain achieved by the channelized matching circuit. Although the deep null between 140 and 300 MHz is filled, the antenna is still poorly matched.

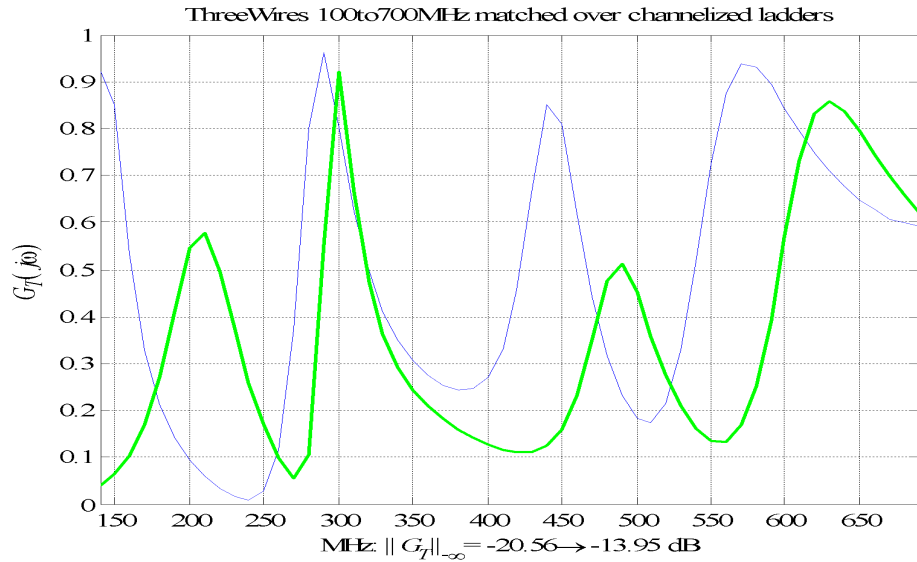


Figure 24: Channelized 2-ports (shunt inductance)

Searching over several classes of lumped ladders for better performance was fruitless. This empty search offers two lessons. First, time and effort can be wasted without good matching bounds. Such bounds can show a design is simply not feasible and a fruitless search is avoided. Second, the non-reactive matching obtained by the degree $d = 0$ multiports shows that simply throwing lots of lumped elements at the problem is futile—if only channelized matching is used. Rather, some cross coupling must be present. Accordingly, the topology was slightly generalized.

Figure 25 shows a power trivider consisting of channelized 2-ports with admittance matrices Y_B , Y_C , and Y_D that all terminate in a common 2-port with admittance matrix Y_A .

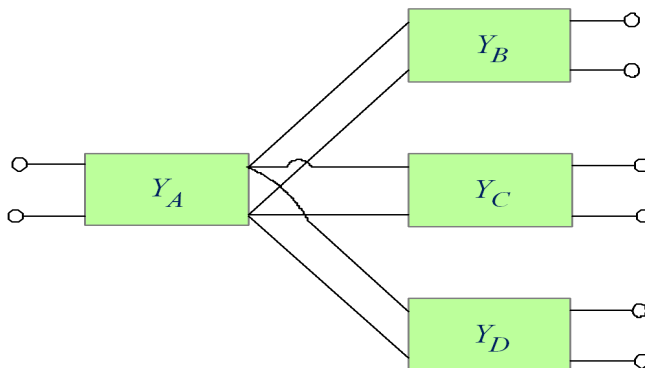


Figure 25: Power trivider.

For matching, the 2-ports are ideal transmission lines. A uniform, lossless transmission line of characteristic impedance z_c and *commensurate* length ℓ is called a *unit element* (UE) and has a *chain matrix* [4, Eq. 8.1]

$$T_{\text{UE}}(p) = \begin{bmatrix} \cosh(\tau p) & z_c \sinh(\tau p) \\ y_c \sinh(\tau p) & \cosh(\tau p) \end{bmatrix},$$

where $\tau = c^{-1}\ell$ is the commensurate one-way delay determined by the speed of propagation c . Figure 26 shows that this transmission-line topology does slightly better than no matching. The blue line is the gain of the unmatched gain of Figure 14. The green line is the gain provided by the matching circuit. The box lists the impedances z_c 's in ohms and the length in millimeters.

Just as in the multiport matching of Section 5, better performance is obtained by reducing the frequency range. Figure 27 shows pulls in both the high and low ends to obtain a 3.1 VSWR over 300–600 MHz. The high performance obtained at the 600 MHz suggests that the high-frequency range can be extended with a small increase in the VSWR. Likewise, the increasing gain at the low end also suggests that the peak just below 300 MHz can also be exploited.

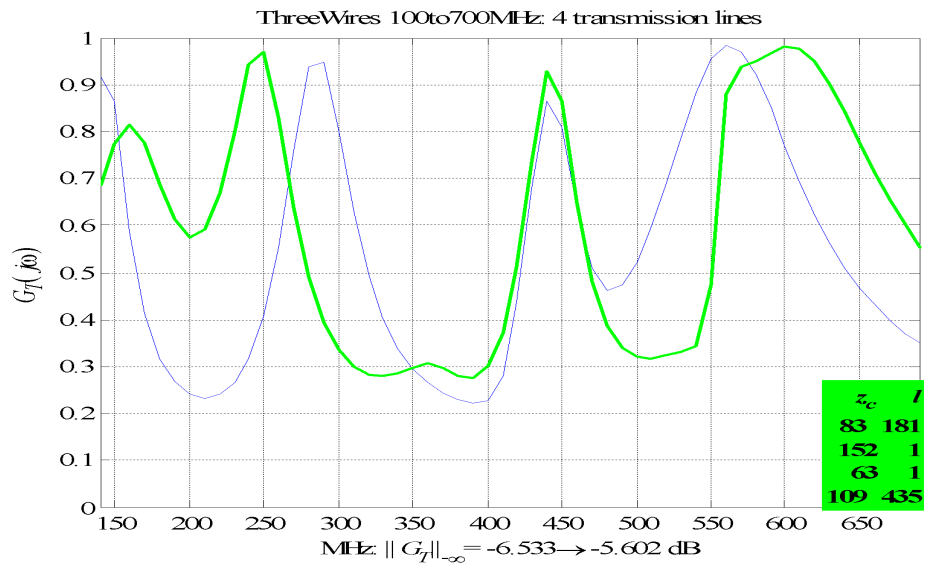


Figure 26: Power trivider matching 140–700 MHz.

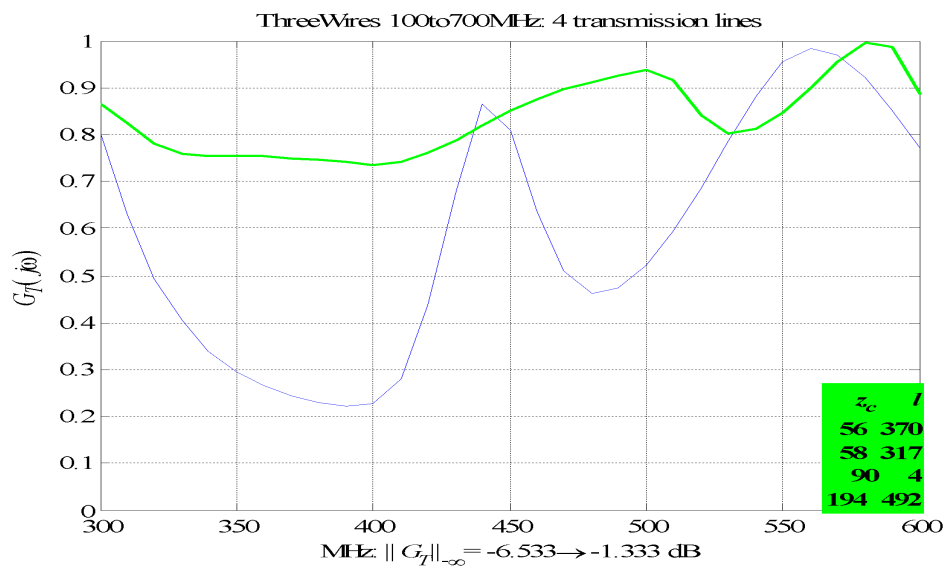


Figure 27: Power trivider matching 300–600 MHz.

Figure 28 verifies the observations of the preceding plots by extending the matching over 270–700 MHz. The VSWR increases from 3.1 to 3.5. What this example does show is that an explicit matching 4-port can deliver some performance. Nevertheless, this approach is still incremental in the sense that cross coupling is not designed into this topology.

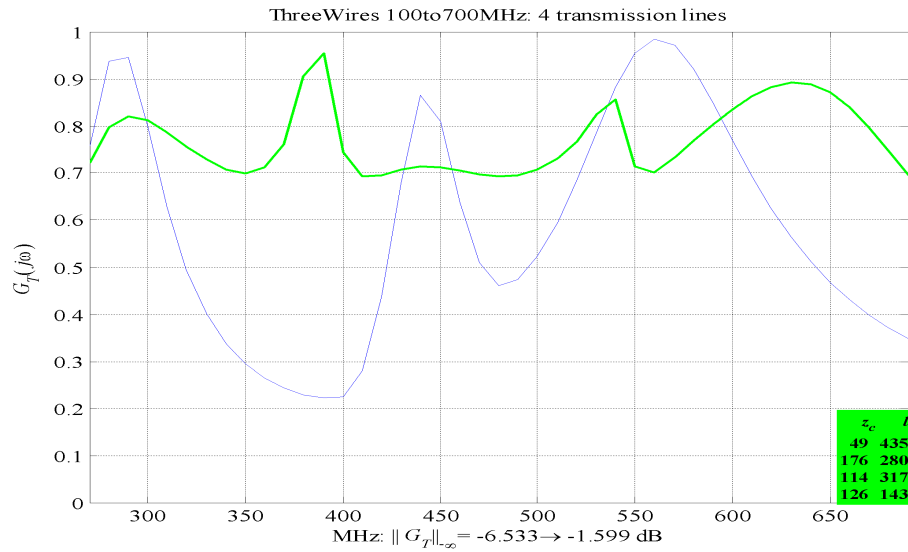


Figure 28: Power trivider matching 270–700 MHz.

7 Exploiting Multiport Coupling

This multiport antenna is an excellent demonstration of the design potential of multiport matching. Exploiting this “lucky hit” has immediate payoffs for theory, multiport design, and optimization. Rather than list a series of “research directions” that constrain cogitation, the following questions are offered in the spirit of using this remarkable multiport matching result for several points-of-departure.

7.1 What are the theoretical limits of multiport matching?

This general question can be focused to ask: Given a multiport load, can the H^∞ bounds or the Fano bounds be computed for the SIMO matching problem? Answering either theoretical question has an immediate practical payoff because unworkable designs can be eliminated without wasting time on fruitless searches [29].

The Fano bounds are basic to single-port matching. A multiport generalization was obtained in 1984 by Wang and Chen [40]. Since then, the Fano literature shows limited development for multiports and is still restricted to rational-function models.

The H^∞ bounds are basic to optimization over analytic functions, or equivalently, to matching circuits. Characteristic of the H^∞ bounds is the “flatness” of the objective function at a local optima: **Helton observed that the flatness and the winding number characterize local optima [21, Theorem 9.3.1]**. In this context, the observed flatness in Figure 17 provides graphical evidence of a theoretically optimal match.

Further consideration of the SIMO question also reveals new approaches to constrained H^∞ optimization. Section 5 sets out the SIMO matching problem for N -port loads S_L as

$$\sup\{\|G_T(s_G, S, S_L)\|_{\Omega, -\infty} : S \in \mathfrak{S}\},$$

where \mathfrak{S} is the class of designable $(N + 1)$ -ports. If the circuit designer is searching for optimal matching from lumped, lossless multiports of degree not exceeding d , the set inclusion

$$\mathfrak{S} \subseteq U^+(N + 1, d),$$

implies the inequality:

$$\begin{aligned} & \sup\{\|G_T(s_G, S, S_L)\|_{\Omega, -\infty} : S \in \mathfrak{S}\} \\ & \leq \sup\{\|G_T(s_G, S, S_L)\|_{\Omega, -\infty} : S \in U^+(N+1, d)\}. \end{aligned}$$

Because $U^+(N+1, d)$ is a subset of H^∞ , several H^∞ techniques can compute upper bounds on this gain. One upper bound follows from maximizing the gain for over the unit ball in H^∞ :

H^∞ SIMO Matching: Given the generator's reflectance s_G and an N -port load $S_L(p)$, maximize the transducer power gain

$$\text{maximize: } \|G_T(s_G, S, S_L)\|_{\Omega, -\infty},$$

where S is an H^∞ function of norm $\|S\|_\infty \leq 1$.

Helton solved this multiport matching problem in his 1981 paper [20, Test IV]. Helton's multiobjective optimization program can also solve this problem [22]. The idea is to compute the Pareto front constructed of the gain and multiport norm. This Pareto front subsumes the preceding H^∞ SIMO matching as a special case. Consequently, comparing both methods applied to multiport matching is an excellent research topic.

More attuned to *Lagrange multipliers* is the following constrained optimization problem:

$$\text{maximize: } \|G_T(s_G, S, S_L)\|_{\Omega, -\infty}$$

subject to the constraints that S is an H^∞ function of unit norm:

$$\|I - S^H S\|_\infty = 1.$$

A reasonable conjecture is that the gradient alignment conditions of the Lagrange multipliers have an analog in H^∞ optimization. Regardless of the methods, computing best possible bounds for multiport matching provides a fundamental benchmark to assess practical design. However, there remains the hard problems of actually synthesizing optimal and near-optimal matching multiports.

7.2 What are the optimal multiport matching circuits?

Figures 17–21 show near-optimal matching performance of the lumped, lossless 4-ports. Consequently, the extraction of a circuit from these near-optimal multiports is a practical problem of synthesis. One approach is the partial-fraction or Foster expansion. Although the Foster expansion does produce a multiport circuit, these circuits are not practical because they are infested with transforms and gyrators—the value of this approach is to demonstrate feasibility [35]. Therefore, other approaches to extract a practical circuit from these lumped, lossless 4-ports are credible lines of research. The payoff from these considerations have immediate applications: antenna matching [34], amplifier design, and circulator optimization [45].

Specific to the three-wire antenna, the multiports need only a few lumped elements to get a good match. In particular, the multiport of Figure 21 has no lumped elements. Its associated scattering matrix is constant and listed in Section 5. Decompositions of this constant scattering matrix may reveal the basic connections between the ports [28, Section 7-2] or relate to the decoupling algorithms of Volmer [37].

7.3 How effective is decoupling?

Figure 1 illustrates the decoupling algorithm [37]. The idea is excellent—use the eigenvectors of the load’s scattering matrix to decouple the multiport load into a collection of single-port loads. The key word in the question is “effective” because problems exist with synthesizing the decoupling circuit over wide frequency band. The basic idea starts with the observation that if S_L is an N -port that diagonalizes as

$$\Lambda = \text{diag}(\lambda_1, \lambda_2, \dots, \lambda_N) = U^T S_L U,$$

where U is an $N \times N$ unitary matrix, the $2N$ -multiport

$$S_U = \begin{bmatrix} 0 & U^T \\ U & 0 \end{bmatrix},$$

is both lossless and decouples the load in cascade:

$$\Lambda = \mathfrak{F}(S_U, S_L) = U^T S_L U.$$

The technical point of this technique is to synthesize the decoupler. Volmer’s approach uses the 2-port directional couplers to synthesize S_U similar to the

way Givens rotations can diagonalize a matrix. This decoupling technique is found in other multiport applications. For example, Czawka [10] offers broadband microstrip uncouplers for multiport complex loads. Closely allied with this SIMO design is a six-channel wideband power divider by Czawka [11]. Jarmasz and Martens [24] apply a variant of this decoupling approach to wave digital filters. Finally, Cameron and Yu [6] offer several multiplexer topologies that can be applied to decoupling design. For example, a wideband decoupler may be obtained by channelizing several narrowband decouplers across the frequency band.

7.4 What are the multiport ladder circuits?

The lossless ladders are basic to 2-port matching. Each ladder's stage commonly consists of a series or shunt element. The stages are cascaded to make a ladder of specified degree. By increasing the degree of the ladder, the matching performance of the ladder's topology (low-pass, high-pass) as a function of degree can be benchmarked against the H^∞ bounds [1]. Therefore, generalization of these 2-port ladders to multiport ladders is a credible research topic with immediate and practical payoffs. As illustrated in Figure 29, one multiport generalization uses a stage consisting of shunts between ports [31], [8]. Just as Fujisawa obtained deep results on characterizing the mid-series and mid-shunt ladders [4], and as Fialkow pushed this program to parallel ladders [16], an analogous multiport ladder program that builds on these classic results awaits the determined researcher.

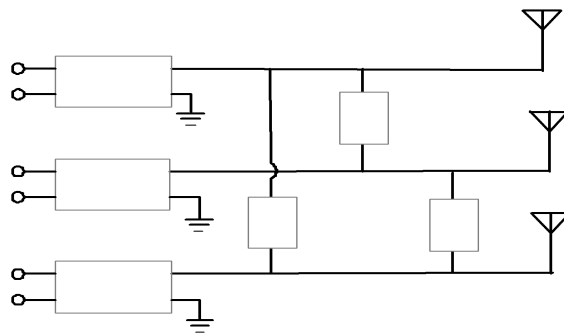


Figure 29: Shunts between ports.

7.5 How critical is multiport matching for MIMO?

Figure 30 illustrates multiport matching in Multiple-Input Multiple-Output (MIMO) systems. Although maximum power transfer is the standard matching objective, MIMO system performance may be enhanced more by decoupling the antenna rather than power matching.

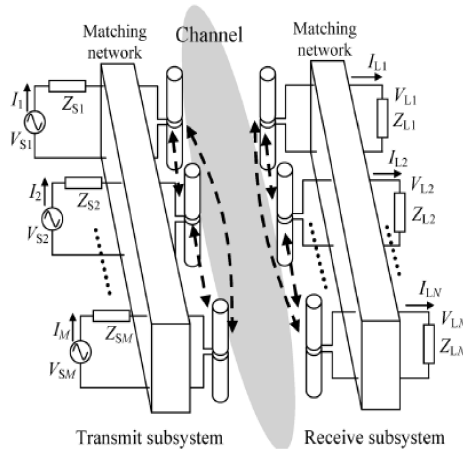


Figure 30: MIMO matching networks [25] © IEEE 2006.

Fei, Fan, and Thompson offer a “multi-handed” discussion of MIMO matching [17]:

...integration of MIMO technique into compact devices is restricted if the antenna spacing is below half a wavelength. This because strong mutual coupling (MC) between closely spaced antenna elements results in changes in antenna patterns (antenna correlation) and loss of antenna efficiency ...MC is claimed as a detriment to MIMO systems. However, MC can also be a positive factor to increase the MIMO performance under some circumstances.

These contrapuntal arguments were addressed by Wallace and Jensen [39] showing MIMO capacity matching is optimized by conjugate matching. However, Fei, Fan, and Thompson also observe that [17]:

...it is not feasible to integrate this solution [conjugate-match] into MIMO systems as multi-loads has to be introduced to each

receive port . . . Although the design of multiport-conjugate matching network has been reported in . . . the authors do not know of any experimental results being presented in the literature. As a result, the single-port match is still an attractive if suboptimal solution

The upshot is that single-port matching is a credible benchmark for proposed multiport matching—any MIMO matching scheme must beat this suboptimal performance. The upper bound for MIMO matching is the conjugate matching [39]. Consequently, there are excellent multiport design opportunities in wideband MIMO. Finally, other multiport design issues arise when transmit and receive technologies are integrated into small systems. Quoting from Morris and Jensen [26]:

As adoption of MIMO technology increases, there will be increased desire to integrate multiple receiver front ends on a single chip, particularly for mobile equipment. As this integration occurs, circuit level signal coupling will increase, potentially leading to altered signal correlation characteristics and signal-to-noise ratio (SNR) at the front end amplifier outputs.

Figure 31 shows a multiport embedded in an active MIMO system. Morris and Jensen show that multiport matching can reduce the electromagnetic signal coupling in the radio receiver front end. Because the amplifiers will introduce gain, noise, and stability problems, *scalar-valued* multiport optimization turns into *vector-valued* multiport optimization and the computation of the associated Pareto fronts.

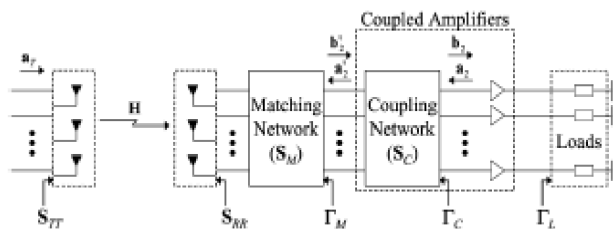


Figure 31: MIMO receiver and matching network [26] © IEEE 2005.

7.6 Multiport Antenna System Optimization

Up to this last example, multiport matching has been focused on matching the 3-port load as a black box rather than as an antenna. This subsection considers the performance of the antenna system both “in the wires” and “over-the-air.” That is, the matching multiport and the antenna’s geometry are simultaneously twiddled to optimize system performance. For example, Czawka and Garbaruk [12] offer a design framework to control the radiation pattern from a multiport antenna by using a lossless multiport to control phase of the feeds. A fast and generalized antenna code is critical to the optimization of such an *antenna system* [7].

Figure 32 illustrates such a system optimization and blurs the distinction between the matching circuit and the antenna. The antenna is still the three-wire antenna. The antenna system is driven by wire #1 fed through its matching 2-port S_1 . The short wire #2 and the long wire #3 are fed by electromagnetic coupling. These two wires are loaded at their feed points with 2-ports with scattering matrices S_2 and S_3 . The design variables are the three 2-ports—and the parameters of the wires: their lengths and spacings. The design problem is to simultaneously match while sweeping over this family of three-wire antennas.

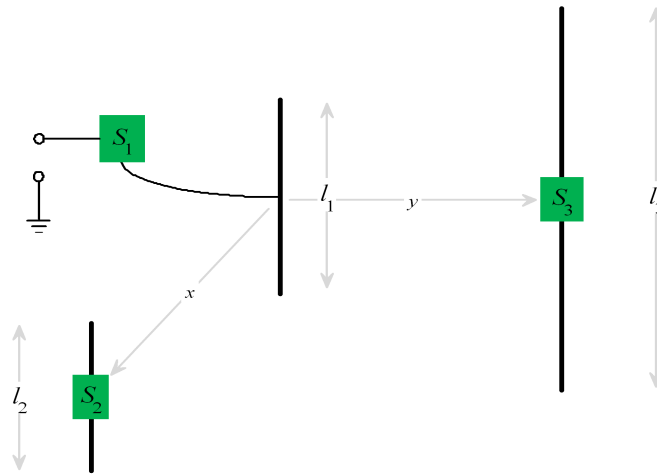


Figure 32: Antenna system (single feed, port loading).

One optimization problem is solved by computing a Pareto front that shows the tradeoff between gain and bandwidth. A more ambitious opti-

mization problem is solved by computing a Pareto surface that shows the tradeoffs between gain, bandwidth, and volume. If a radiation pattern is also specified, the optimization problem is solved by computing the Pareto surface that shows the tradeoffs between gain, bandwidth, and volume—under the constraint that the resulting radiation pattern is within tolerance. A handy “rule-of-thumb” in optimization theory is that any constraint is really an objective function. Consequently, the final antenna design problem is computation of the Pareto surface showing the tradeoffs between gain, bandwidth, volume, and quality of pattern match. Clearly, a fast multi-physics code is needed to handle the lumped elements in the circuit and the distributed electromagnetic performance of the antenna.

References

- [1] Allen, J. C. and Dennis Healy [2003] Nehari's Theorem and Electric Circuits, in *Modern Signal Processing*, Edited by Daniel Rockmore and Dennis Healy, Springer-Verlag.
- [2] Anderson, Brian D. O. [1973] Minimal Gyrator Lossless Synthesis, *IEEE Transactions on Circuit Theory*, CT-20(1), pages 11–15.
- [3] Austin, Brian A. and Kevin P. Murray [1998] The Application of Characteristic-Mode Techniques to Vehicle-Mounted NVIS Antennas *IEEE Antennas and Propagation Magazine*, 40(1).
- [4] Baher, H. [1984] *Synthesis of Electrical Networks*, John Wiley & Sons, New York, NY.
- [5] Balabanian, Norman and Theodore A. Bickart [1981] *Linear Network Theory*, Matrix Publishers, Inc., Beaverton, OR.
- [6] Cameron, Richard J. and Ming Yu [2007] Design of Manifold-Coupled Multiplexers, *IEEE Microwave Magazine*, 10, pages 46–59.
- [7] Champagne, N. J., D. R. Wilton, J. D. Rockway [2006] The Analysis of Thin Wires Using Higher-Order Elements and Basis Functions, *IEEE Transactions on Antennas and Propagation*, 54(12), pages 3815–3821.
- [8] Chua, Ping Tyng and Jacob Carl Coetzee [2005] Microstrip Decoupling Networks For Low-order Multiport Arrays With Reduced Element Spacing, *Microwave And Optical Technology Letters*, 46(6).
- [9] Coetzee, Jacob C. and Yantao Yu [2008] Port Decoupling for Small Arrays by Means of an Eigenmode Feed Network, *IEEE Transactions on Antennas and Propagation*, 56(6).
- [10] Czawka, G. [2002] Synthesis of Broadband Microstrip Uncouplers for Multiport Complex Loads, *14th International Conference on Microwaves, Radar and Wireless Communications, MIKON-2002*, Volume 1, pages 55–58.

- [11] Czawka, G. and N. Litwińczuk [2004] Six-Channel Broadband Inhomogeneous Microstrip Power Divider for Communication Antenna Array, *15th International Conference on Microwaves, Radar and Wireless Communications, MIKON-2004*, Volume 3, pages 1020–1023.
- [12] Czawka, Giennadij and Marek Garbaruk [2004] Frequency and Time Simulation of Electromagnetic Field of Microwave Antenna Array, *15th International Conference on Microwaves, Radar and Wireless Communications, MIKON-2004*, Volume 2, pages 469–472.
- [13] Dewilde, Patrick [1999] Generalized Darlington Synthesis, *IEEE Transactions on Circuits and Systems-I*, 45(1).
- [14] Dobrowolski, Janusz A. and Wojciech Ostrowski [1996] *Computer-Aided Analysis, Modeling, and Design of Microwave Networks*, Artech House, Boston, MA.
- [15] Douglas, R. G. & J. W. Helton [1973a] The Precise Theoretical Limits of Causal Darlington Synthesis, *IEEE Transactions on Circuit Theory*, CT-20 (3), page 327.
- [16] Fialkow, Aaron D. [1979] Inductance, Capacitance Networks Terminated in Resistance, *IEEE Transactions on Circuits and Systems*, Volume CAS-26, Number 8, pages 603–641.
- [17] Fei, Yuanyuan, Yijia Fan and John S. Thompson [2007] Optimal Single-Port Impedance Matching for Compact MIMO Arrays, *IEEE GLOBECOM 2007 Proceedings*.
- [18] Gonzalez, Guillermo [1997] *Microwave Transistor Amplifiers*, Second Edition, Prentice Hall, Upper Saddle River, NJ.
- [19] Harrington, Roger F. and Joseph R. Mautz [1971] Computation of Characteristic Modes for Conducting Bodies, *IEEE ASSP*, AP-19(5).
- [20] Helton, J. William [1981] Broadbanding: Gain Equalization Directly from Data, *IEEE Transactions on Circuits and Systems*, CAS-28(12).
- [21] Helton, J. W. and O. Merino [1998] *Classical Control Using H^∞ Methods*, SIAM, Philadelphia.

- [22] Helton, J. William and Andrei E. Vityaev [1997] Analytic functions optimizing competing constraints *SIAM Journal on Mathematical Analysis*, 28(3), pages 749–767.
- [23] Hazdra, Pavel, Pavel Hamouz, Miloš Mázanek, Stanislav Zvánovec [2007] Theory of Characteristic Modes: Getting More Insight into Linear Antenna Behavior *17th International Conference of Radioelektronika*, page 1–4.
- [24] Jarmasz, M. R. and G. O. Martens [1987] Design of Canonic Wave Digital Filters Using Brune and Matched 4-Port Adaptors, *IEEE Transactions on Circuits and Systems*, CAS-34(5).
- [25] Lau, Buon Kiong, Jorgen Bach Andersen, Gerhard Kristensson, and Andreas F. Molisch [2006] Impact of Matching Network on Bandwidth of Compact Antenna Arrays, *IEEE Transactions on Antennas and Propagation*, 54(11).
- [26] Morris, Matthew L. and Michael A. Jensen [2005] Impact of Receive Amplifier Signal Coupling on MIMO System Performance, *IEEE Transactions on Vehicular Technology*, 54(5).
- [27] Neiryntik, Jacques and Charles-Henri Carlin [1981] Synthesis of the Lossless reciprocal Three-Port Based on a Canonic Form of Its Scattering Matrix, *IEEE Transactions on Circuits and Systems*, CAS-28(7).
- [28] Newcomb, Robert W. [1966] *Linear Multiport Synthesis*, McGraw-Hill Electronic Sciences Series, New York, NY.
- [29] Nordebo, S. Gustafsson, M. [2005] Multichannel Broadband Fano Theory for Arbitrary Lossless Antennas with Applications in DOA Estimation, *IEEE International Conference on Acoustics, Speech, and Signal Processing, (ICASSP '05)*, Volume 4, pages iv/969–iv/972.
- [30] Oono, Yoisiro [1972] Minimum-Gyrator Synthesis of n -Ports, *IEEE Transactions on Circuit Theory*, CT-19(4), pages 313–316.
- [31] Riblet, Gordon P. [1985] Broad-Band Internally and Externally Matched Lumped Element Symmetrical 5-Ports, *IEEE Transactions on Circuits and Systems*, CAS-32(12).

- [32] Rockway, J. W. and J. Logan [1999] *Expert MININEC Broadcast Professional for Windows*, EM Scientific, Inc., Carson City, NV.
- [33] Rockway, J. W. and J. Logan [1995] Advances in MININEC, *IEEE Antennas and Propagation Magazine*, 37(4), pages 7–12.
- [34] Schwartz, David F. and J. C. Allen [2004] Wideband Impedance Matching: H^∞ Performance Bounds, *IEEE Transactions on Circuits and Systems II: Express Briefs*, 51(7), pages 364–368.
- [35] Temes, Gabor C. and Jack W. LaParta [1977] *Circuit Synthesis and Design*, McGraw-Hill Inc., New York, NY.
- [36] www.antennamodel.com
- [37] Volmer, Christian, Jörn Weber, Ralf Stephan, Kurt Blau, Matthias A. Hein [2008] An Eigen-Analysis of Compact Antenna Arrays and Its Application to Port Decoupling, *IEEE Transactions on Antennas and Propagation*, 56(2).
- [38] Wallace, Jon W. and Michael A. Jensen [2004] Termination-Dependent Diversity Performance of Coupled Antennas: Network Theory Analysis, *IEEE Transactions on Antennas and Propagation*, 52(1).
- [39] Wallace, Jon W. and Michael A. Jensen [2004] Mutual Coupling in MIMO Wireless Systems: A Rigorous Network Theory Analysis *IEEE Transactions on Wireless Communications*, 3(4).
- [40] Wang, Zhao-Ming, Wai-Kai Chen [1984] Broad-Band Matching of Multiport Networks, *IEEE Transactions on Circuits and Systems*, CAS-31(9).
- [41] Weber, Jörn, Christian Volmer, Kurt Blau, Ralf Stephan, Matthias A. Hein [2006] Miniaturized Antenna Arrays Using Decoupling Networks With Realistic Elements, *IEEE Transactions on Microwave Theory and Techniques*, 54(6).
- [42] Wohlers, M. Ronald [1969] *Lumped and Distributed Passive Networks*, Academic Press, New York, NY.
- [43] Yaghjian, Arthur D. and Steven R. Best [2005] Impedance, Bandwidth, and Q of Antennas, *IEEE Transactions on Antennas and Propagation*, 53(4).

- [44] Youla, Dante C. [1971] A Tutorial Exposition of Some Key Network-Theoretic Ideas Underlying Classical Insertion-Loss Filter Design, *Proceedings of the IEEE*, Volume 59, Number 5, pages 760–799.
- [45] Young, J. L., R. S. Adams, B. O’Neil, C. M. Johnson [2006] Bandwidth Optimization of an Integrated Microstrip Circulator and Antenna Assembly, *IEEE Antennas and Propagation Magazine*, 48(6), pages 47–56.

A Characteristic Modes of the Three-Wire Antenna

Because the coupling between the ports of the three-wire antenna gives its wideband performance, the discussion of Section 3 is augmented by this appendix. The characteristic modes reveal the resonances and couplings of the three wires. Figure A-1 re-plots the three wires for the reader's convenience.

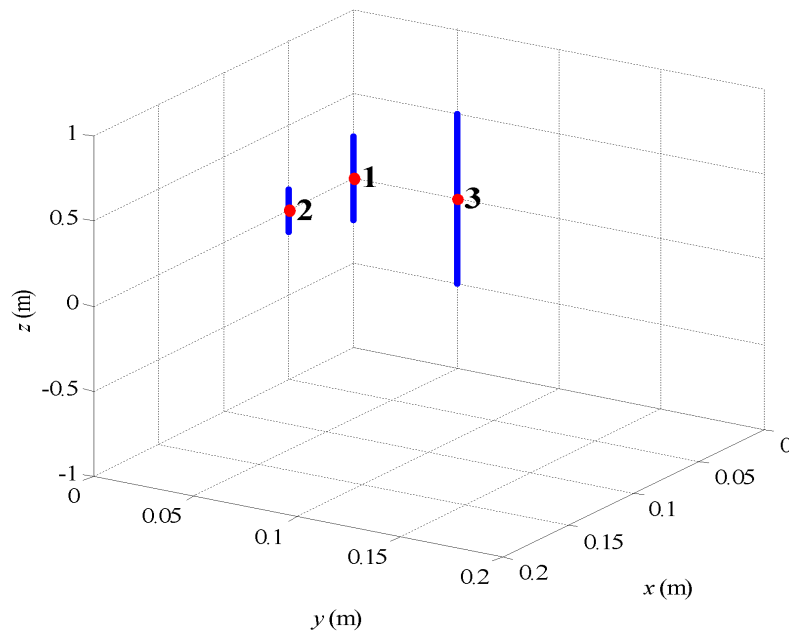


Figure A-1: Center-fed Dipoles: 1/4, 1/2, and 1 meter in length

Figure A-2 displays the impedance matrix determined by the segmenting of the wires as listed in Table 3. The matrix breaks into three blocks corresponding to the three wires. The blocks on the main diagonal show the coupling between the segments on a wire. The off-diagonal blocks show the impedance coupling between the wires. Write the impedance matrix using its real and imaginary parts:

$$Z = R + jX.$$

The resistance and reactance are real matrices, with $R \geq 0$. Make the assumption that the segmentation is sufficiently homogenous so that these real

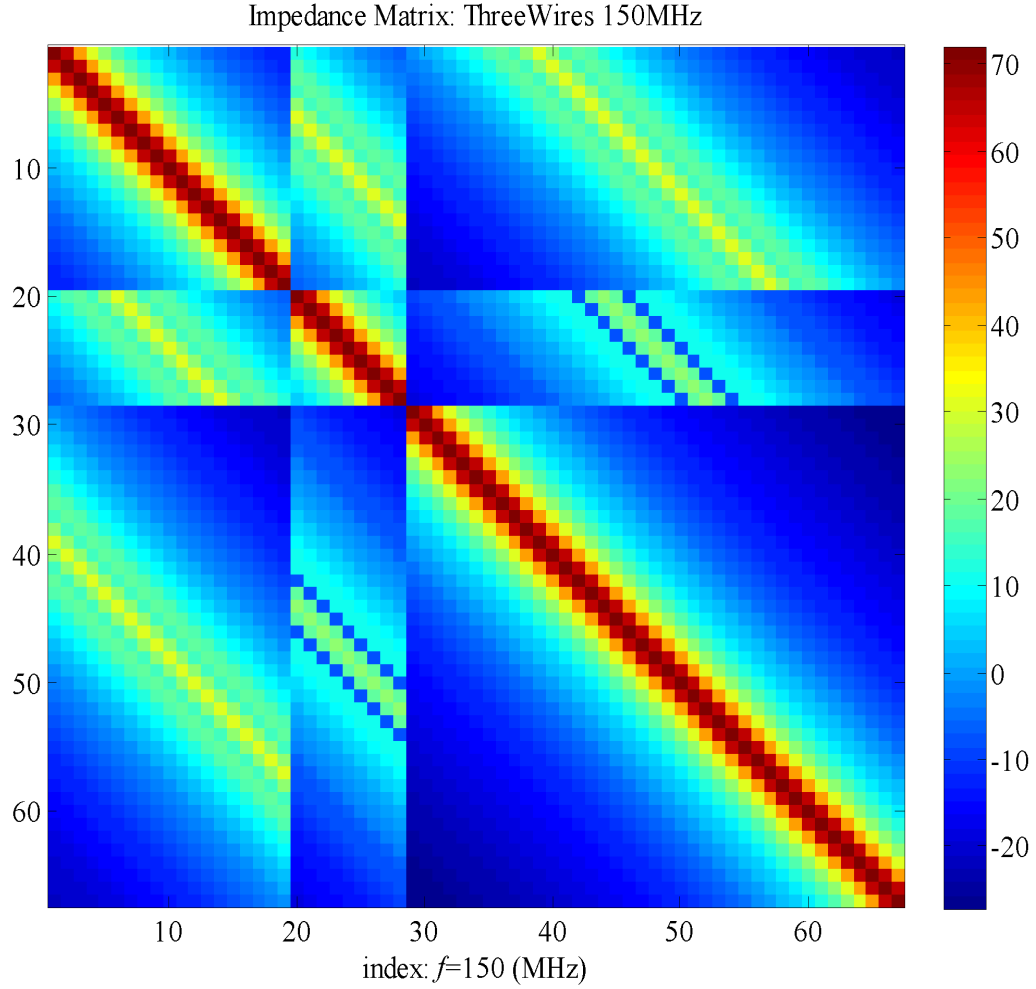


Figure A-2: Impedance matrix at 150 MHz.

matrices are also symmetric. The *characteristic modes* are the eigenvalues of [19]:

$$XJ = RJA; \quad \Lambda = \text{diag}(\lambda_1, \dots, \lambda_N),$$

where J is matrix of eigencurrents. Because X and R are real and symmetric, Λ must be real. If R is invertible ($R > 0$), replace $J = R^{-1/2}W$ to get

$$R^{1/2}XR^{-1/2}W = W\Lambda.$$

This ordinary eigenvalue problem admits a solution W that is real and orthonormal: $I = W^T W$. Consequently, the eigencurrents J are orthonormal with respect to the resistance matrix:

$$J^T R J = I.$$

A physical meaning of the characteristic modes follows from the impedance matrix

$$Z J = R J (I + j \Lambda).$$

Resonance is said to occur when a characteristic mode vanishes [23]: $\lambda_n = 0$. If $\lambda_n > 0$, its eigencurrent \mathbf{j}_n is said to make an *inductive* contribution. If $\lambda_n < 0$, its eigencurrent \mathbf{j}_n is said to make a *capacitive* contribution. Properties of the eigencurrents are offered by Austin and Murray [3]:

An important property of these current modes is that they are orthogonal over the surface, as are the fields that they produce over the sphere at infinity, and so they radiate power independently of one another. The magnitude of λ_n denotes the relative significance of each mode, in terms of the ratio of stored energy to radiated power. The closer $|\lambda_n|$ is to zero, and hence to resonance, the more substantial is its contribution to the overall radiation.

If these modes can be individually excited by an adroit placement of feed points, design of antennas and shaping of radiated fields follows from the orthogonality of the eigencurrents. The following plots illustrate these concepts.

Figure A-3 plots the two most radiating eigencurrents at 150 MHz. Because the wire segments are the same lengths and the indices run along the wires, the plot shows the current along the wires. The half-wave resonance of the long wire with a characteristic mode of $\lambda = 0.61187$ (blue curve). Most of the current resides on the long wire but there is current on both the shorter wires. Comparison with Figure 6 reveals 150 MHz is slightly above resonance of the long wire. Consequently, the characteristic mode is slightly positive rather than zero. If a feed point is placed at the center of the long wire, this mode could be excited at 150 MHz and radiate most of its power. Figure A-3 also plots the next most radiative eigencurrent ($\lambda = -143$) that corresponds to the full-wave resonance of the long wire. If feed points are placed at the extrema of this eigencurrent, this mode will be excited (with opposite phasing) at 150 MHz. However, the radiation from this eigencurrent with $\lambda = -143$ is relatively small.

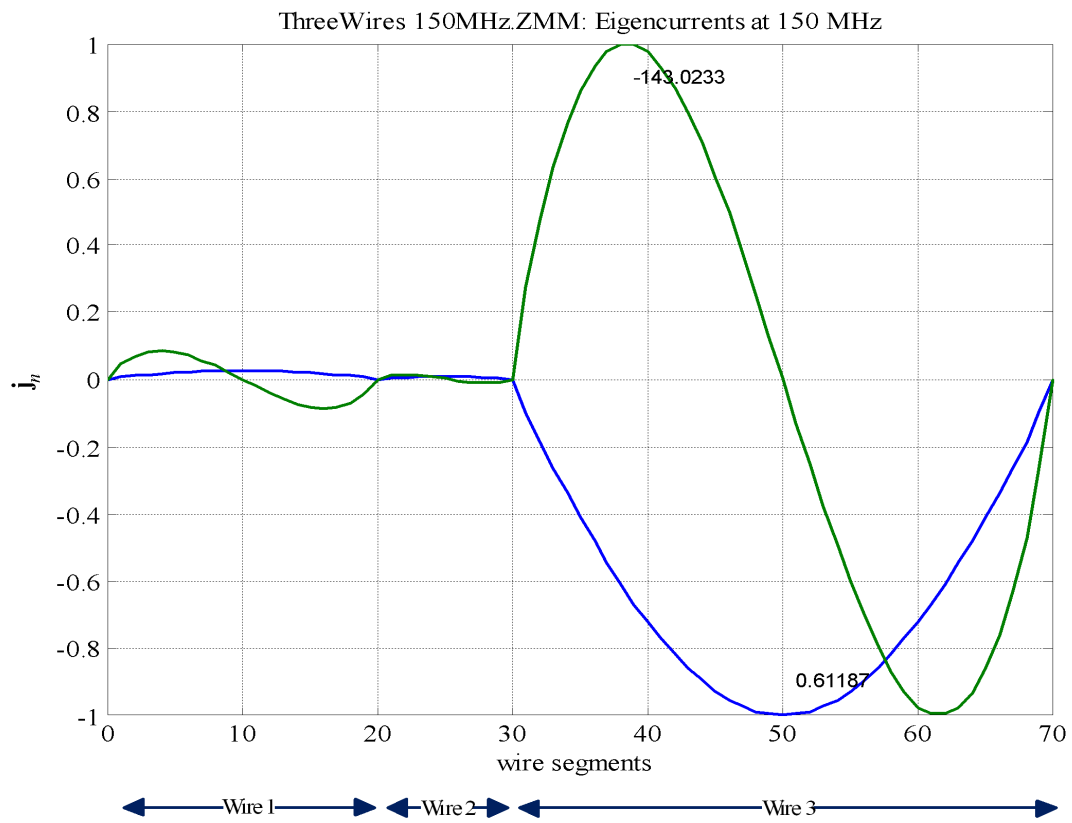


Figure A-3: Eigencurrents at 150 MHz.

Figure A-4 plots two significant eigencurrents at 300 MHz. The medium-length wire does show half-wave resonance ($\lambda = 0.65159$) and shows coupling into the other wires. However, the most efficient resonance ($\lambda = 0.47758$) is the full-wave resonance of the long wire (blue line). Thus, 300 MHz is slightly above resonance for both the long and medium-length wires. A feed point placed at the center of the medium-length wire should excite this mode. Two feed points on the long wire and oppositely phased should drive the full-wave resonance. Weighting and phasing these two eigencurrents allows some beamforming in the far field.

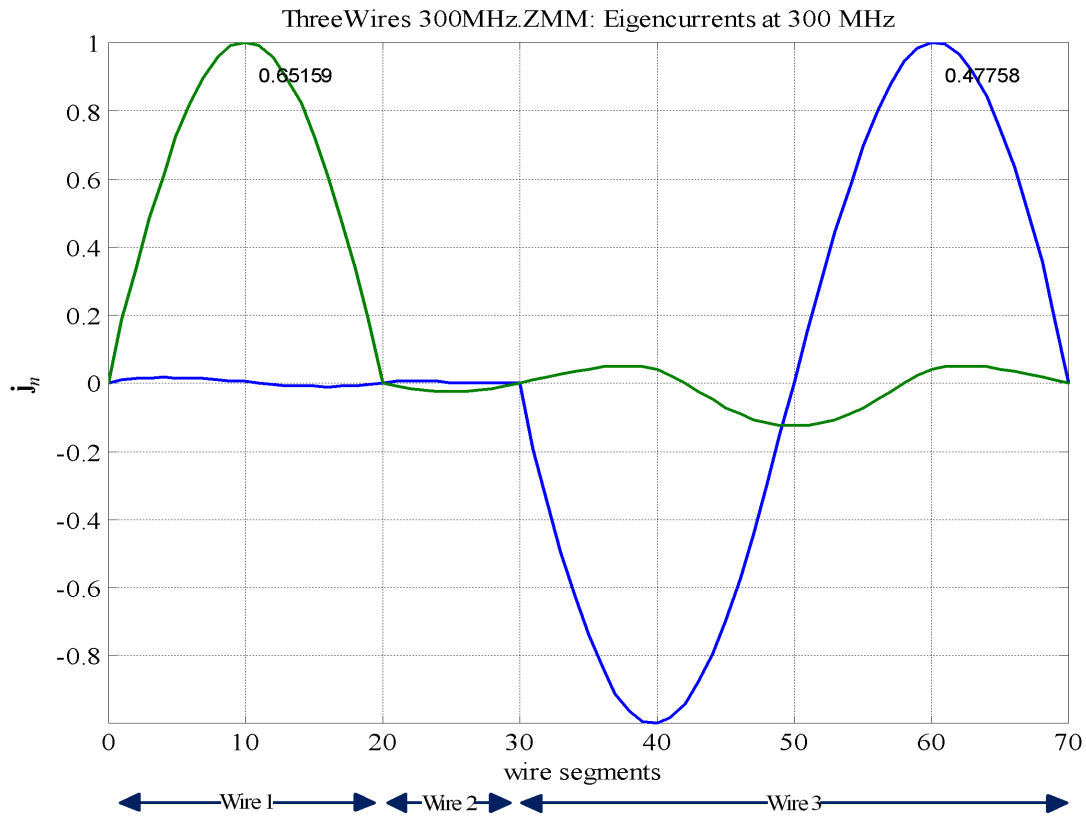


Figure A-4: Eigencurrents at 300 MHz.

Figure A-5 plots three significant eigencurrents to 600 MHz: the half wave on the short wire, the full wave on medium-length wire, and the two waves on the long wire. This plot reveals some interesting feed-point design problems with respect to exciting individual modes. A single feed centered on the short wire should only excite its half wave ($\lambda = 0.45367$). Two feeds on the medium-length wire ($\lambda = 0.44225$) produce the full-wave on that wire and two waves on the long wire. Likewise, four feeds on the long wire should excite the two-wave current ($\lambda = 0.21943$). Thus, a total of seven feeds should allow control of these three eigencurrents and the associated orthogonal decomposition of the far field.

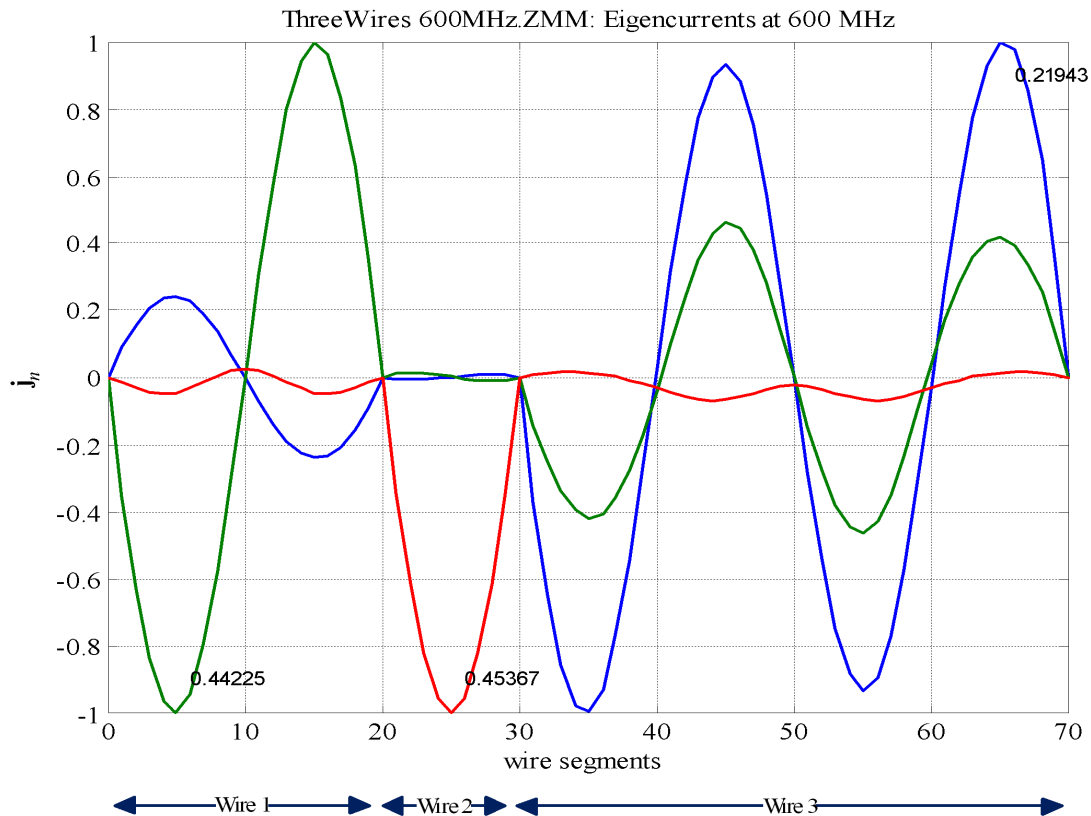


Figure A-5: Eigencurrents at 600 MHz.

Figure A-6 shows significant eigencurrents at 450 MHz. The plot reveals that the three-wire antenna is radiating from the long wire ($\lambda = 0.36559$) with $3/2$ wave. The extrema of this wave should set the location of the feeds on the long wire. However, the λ values of the other eigencurrents show radiation at 450 MHz could be accomplished from several locations.

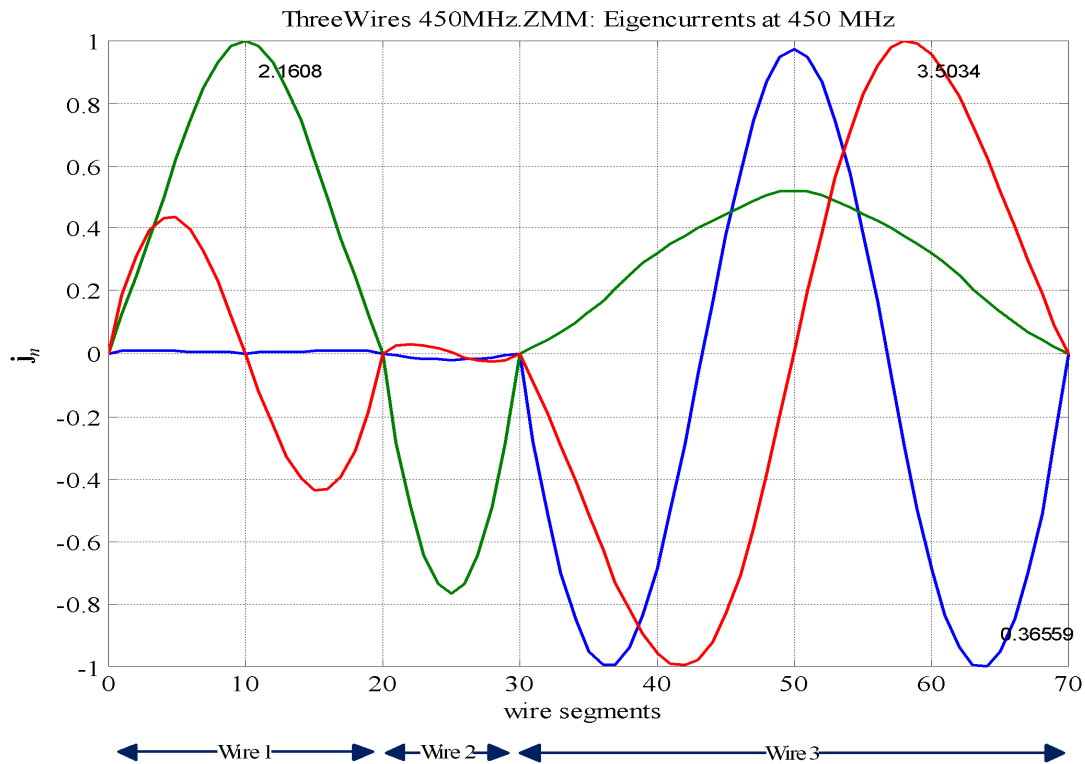


Figure A-6: Eigencurrents at 450 MHz.

In summary, these plots demonstrate that the three-wire antenna has several radiation modes, shows the coupling between the wires, locates credible feed points and phasing for this antenna system. Thus, the design insight provided by the characteristic modes by locating these feed points and phasing is orders-of-magnitude more efficient than the “ant-like” combinatorial algorithms that search all segments and phases for such control points. Finally, the design insight provided by the characteristic modes also points to the 2-port loading led to Figure 32 and points to end-to-end loading with low-pass filters for better performance at the lower frequencies.

B Lumped, Lossless N -Ports

Let $U^+(N, d)$ denote the class of lumped, lossless N -ports of degree d . Physically, $U^+(N, d)$ represents *all* the N -ports that can be synthesized with at most d *lumped* elements—inductors and capacitors—connected only by wires, transformers, and gyrators. Excellent wideband matching to the three-wire antenna was obtained from the 4-ports with degree $d \geq 3$. This appendix reviews $U^+(N, d)$ to analyze these matching results.

Mathematically, $U^+(N, d)$ consists of all $N \times N$ scattering matrices $S(p)$ that are real, rational, analytic and bounded on the open right half of the complex plane \mathbb{C}_+ , unitary on the imaginary axis

$$S(j\omega)^H S(j\omega) = I_N,$$

and have Smith-McMillan degree

$$\deg_{\text{SM}}[S(p)] \leq d.$$

The initial results on the Belevitch's Theorem characterizes the scattering matrices for the lumped, lossless 2-ports of $U^+(2, d)$.

A *lumped, passive 2-port* contains the lumped elements—inductors, capacitors, resistors—and the means of connections—wires, transformers, and gyrators. The corresponding scattering matrix [28], [42]

$$S(p) = \begin{bmatrix} S_{11}(p) & S_{12}(p) \\ S_{21}(p) & S_{22}(p) \end{bmatrix}$$

is a rational function that is analytic on the open right half plane \mathbb{C}_+ , satisfies the real condition

$$S(p) = \overline{S(\bar{p})} \quad (p \in \mathbb{C}_+),$$

and is a contraction

$$S(p)^H S(p) \leq \begin{bmatrix} 1 & 0 \\ 0 & 1 \end{bmatrix} \quad (p \in \mathbb{C}_+).$$

A *lumped, lossless 2-port* omits the resistors. As a consequence, its scattering matrix $S(p)$ is a real rational function that is analytic on \mathbb{C}_+ , a contraction on \mathbb{C}_+ , and unitary on the boundary of \mathbb{C}_+ :

$$S(j\omega)^H S(j\omega) = \begin{bmatrix} 1 & 0 \\ 0 & 1 \end{bmatrix}.$$

A *lumped, passive, reciprocal* 2-port omits the gyrators. The associated scattering matrix $S(p)$ is a real rational function that is analytic on \mathbb{C}_+ , and a contraction on \mathbb{C}_+ that is also symmetric:

$$S(p) = S(p)^T \quad (p \in \mathbb{C}_+).$$

Belevitch's Theorem asserts the existence of a scattering matrix $S(p)$ for each 2-port and obtains the converse of these statements.

BELEVITCH'S THEOREM [44], [4, pages 83–86] A lumped, lossless 2-port admits a scattering matrix

$$S(p) = \frac{1}{g(p)} \begin{bmatrix} h(p) & f(p) \\ \epsilon f_*(p) & -\epsilon h_*(p) \end{bmatrix},$$

where $h_*(p) = h(-p)$ and (f, g, h) is a Belevitch triple:

B-1 $f(p)$, $g(p)$, and $h(p)$ are real polynomials; $\epsilon = \pm 1$,

B-2 $g(p)$ is strict Hurwitz (no zeros in the closed right half plane).

B-3 $g_*(p)g(p) = f_*(p)f(p) + h_*(p)h(p)$ for all $p \in \mathbb{C}$.

Conversely, any such $S(p)$ is the scattering matrix for some lumped, lossless 2-port. Moreover, if the 2-port is reciprocal

$$S(p) = \frac{1}{g(p)} \begin{bmatrix} h(p) & f(p) \\ f(p) & -\epsilon h_*(p) \end{bmatrix},$$

where either $f(p)$ is even and $\epsilon = -1$, or $f(p)$ is odd and $\epsilon = 1$. Conversely, any such $S(p)$ is the scattering matrix for some lumped, lossless, reciprocal 2-port.

The number of reactive lumped elements—the inductors and capacitors—is linked to the degree of the 2-port.

Definition 1 [42, page 91]: Let the K distinct poles of $S(p)$ be denoted as p_k . Let $\deg(S(p); p_k)$ denote the largest order to which $p = p_k$ appears in any minor of $S(p)$. The Smith-McMillan degree of $S(p)$ is

$$\deg_{\text{SM}}[S(p)] := \sum_{k=1}^K \deg(S(p); p_k).$$

Belevitch's Theorem characterizes $U^+(2, d)$. The scattering matrices in $U^+(2, d)$ constitute the "state-space" curve in Figure 12. Although Belevitch's Theorem admits some direct extensions [27], the state-space representation is more useful for N -ports. Figure B-1 illustrates the state-space representation of a passive, lumped N -port.

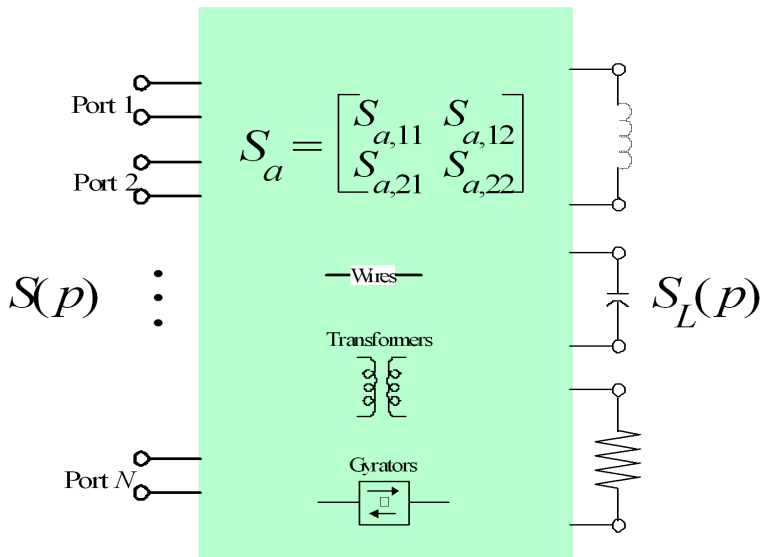


Figure B-1: State-space representation of a passive, lumped N -port.

The figure shows that by pulling the d reactive elements and the r lossy elements into the *augmented load* $S_L(p)$, what is left is an multiport consisting of the wires, transformers, and gytrators with scattering matrix S_a . Because S_a represents a multiport containing only wires, transformers, and gytrators, S_a is a constant matrix. Moreover, because the multiport containing only wires, transformers, and gytrators is lossless, S_a is a constant unitary matrix.

The N -port is obtained by looking into Ports 1, 2, \dots , N of the *augmented scattering matrix* S_a while its remaining ports are terminated in the augmented load $S_L(p)$. That is, $S(p)$ is the image of the augmented load viewed through the augmented scattering matrix S_a . Theorem 1 gives the precise statement of this *state-space representation*.

Theorem 1 (State-Space [42, pages 90–93]) *Every lumped, passive, causal, time-invariant N -port admits a scattering matrix $S(p)$ and conversely. If $S(p)$ has Smith-McMillan degree d and normal rank r , defined as [42, page 91]:*

$$r[S(p)] := \text{rank}[I_N - S(-p)^T S(p)],$$

$S(p)$ admits the state-space representation:

$$S(p) := S_{a,11} + S_{a,12} S_L(p) (I_{d+r} - S_{a,22} S_L(p))^{-1} S_{a,21},$$

where the augmented load is

$$S_L(p) = \begin{bmatrix} q \times I_{N_L} & 0 & 0 \\ 0 & -q \times I_{N_C} & 0 \\ 0 & 0 & 0 \times I_r \end{bmatrix}, \quad \left(q = \frac{p-1}{p+1} \right),$$

and $N_L + N_C = d$. The augmented scattering matrix is

$$S_a = \begin{bmatrix} S_{a,11} & S_{a,12} \\ S_{a,21} & S_{a,22} \end{bmatrix} \begin{matrix} N \\ d+r \\ N \\ d+r \end{matrix},$$

which is a constant, real, orthogonal matrix. If the N -port is lossless, then $r = 0$. If the N -port is reciprocal, then S_a is symmetric, $S_a^T = S_a$.

The power of the state-space representation is that the scattering matrix encodes the structure of the N -port [42, page 91], [28]:

- Any N -port that has $S(p)$ as its scattering matrix contains at least $r[S(p)]$ resistors. Moreover, of all the N -ports that have $S(p)$ as their scattering matrix, at least one has exactly $r[S(p)]$ resistors.
- Let N_L and N_C denote the number of inductors and capacitors in an N -port. For every N -port with scattering matrix $S(p)$, $N_L + N_C \geq \text{deg}_{\text{SM}}[S(p)]$. Moreover, of all the N -ports that have $S(p)$ as their scattering matrix, at least one N -port has exactly this many inductors and capacitors.
- The number of gyrators in any N -port must always exceed the gyrator rank:

$$g[S(p)] := \frac{1}{2} \text{rank}[S(p) - S(p)^T].$$

Oono [30] established that exactly $g[S(p)]$ gyrators are needed to synthesize the N -port. Consequently, when $g[S(p)] = 0$ or when $S(p)$ is symmetric, the N -port is reciprocal and contains no gyrators. Phase 2 of this series will report that excellent wideband matching is still possible using reciprocal multiports. Specifically, good matching is obtained using only capacitors—no inductors and no gyrators.

- Anderson [2] obtains the general result regarding N -port synthesis: an N -port synthesis is possible with $\deg_{\text{SM}}[S(p)]$ reactive elements *and* $g[S(p)]$ gyrators.

Section 5 applies this state-space representation for wideband matching of the three-wire antenna by specializing to the $U^+(4, d)$.

REPORT DOCUMENTATION PAGE

*Form Approved
OMB No. 0704-01-0188*

The public reporting burden for this collection of information is estimated to average 1 hour per response, including the time for reviewing instructions, searching existing data sources, gathering and maintaining the data needed, and completing and reviewing the collection of information. Send comments regarding this burden estimate or any other aspect of this collection of information, including suggestions for reducing the burden to Department of Defense, Washington Headquarters Services Directorate for Information Operations and Reports (0704-0188), 1215 Jefferson Davis Highway, Suite 1204, Arlington VA 22202-4302. Respondents should be aware that notwithstanding any other provision of law, no person shall be subject to any penalty for failing to comply with a collection of information if it does not display a currently valid OMB control number.

PLEASE DO NOT RETURN YOUR FORM TO THE ABOVE ADDRESS.

1. REPORT DATE (DD-MM-YYYY) 09-2008		2. REPORT TYPE Final	3. DATES COVERED (From - To)		
4. TITLE AND SUBTITLE WIDEBAND MULTIPORT MATCHING PHASE I: SINGLE-FEED MULTIPORT ANTENNAS			5a. CONTRACT NUMBER		
			5b. GRANT NUMBER		
			5c. PROGRAM ELEMENT NUMBER		
6. AUTHORS J. C. Allen J. Rockway D. Arceo			5d. PROJECT NUMBER		
			5e. TASK NUMBER		
			5f. WORK UNIT NUMBER		
7. PERFORMING ORGANIZATION NAME(S) AND ADDRESS(ES) SSC San Diego San Diego, CA 92152-5001			8. PERFORMING ORGANIZATION REPORT NUMBER TR 1972		
9. SPONSORING/MONITORING AGENCY NAME(S) AND ADDRESS(ES) Office of Naval Research 800 North Quincy Avenue Arlington, VA 22203-1995			10. SPONSOR/MONITOR'S ACRONYM(S) ONR		
			11. SPONSOR/MONITOR'S REPORT NUMBER(S)		
12. DISTRIBUTION/AVAILABILITY STATEMENT Approved for public release; distribution is unlimited.					
13. SUPPLEMENTARY NOTES This is the work of the United States Government and therefore is not copyrighted. This work may be copied and disseminated without restriction. Many SSC San Diego public release documents are available in electronic format at http://www.spawar.navy.mil/sti/publications/pubs/index.html .					
14. ABSTRACT Impedance matching is a canonical problem in electrical engineering. The problem is to maximize power flowing from a generator to a load with an adroit design of a matching network. Typically, matching problems use a single-port load. In contrast, this report develops matching for a load with multiple ports. The specific multiport load is a three-wire antenna. Each wire has a feed port so that the load is a 3-port. The matching problem is to find a matching network that maximizes power flow from a single feed to all three ports across a wide frequency band (100-700 MHz). Unexpectedly, several theoretical matching multiports were found that gave excellent wideband performance. Consequently, this serendipitous result opens several directions of opportunity. One direction aims at the enhancing the antenna's wideband performance. Understanding the physical phenomenon of coupling between the wires, the physical geometry of the wires, and a Pareto theory for maximal bandwidth and minimal size are all significant research topics. Another direction aims at the matching networks because of the gaps in theory and practical design. Specific and detailed formulation of these research opportunities is made explicit in this report.					
15. SUBJECT TERMS Mission Area: Communications multiport matching wideband frequency channelized multiports port decoupling three-wire antenna Pareto surface					
16. SECURITY CLASSIFICATION OF:			17. LIMITATION OF ABSTRACT	18. NUMBER OF PAGES	19a. NAME OF RESPONSIBLE PERSON
a. REPORT	b. ABSTRACT	c. THIS PAGE			J. C. Allen
U	U	U	UU	64	19b. TELEPHONE NUMBER (Include area code) (619) 553-6566

Approved for public release; distribution is unlimited.